



Variability of projected terrestrial biosphere responses to elevated levels of atmospheric CO₂ due to uncertainty in biological nitrogen fixation

Johannes Meyerholt^{1,2}, Sönke Zaehle^{1,3}, and Matthew J. Smith⁴

¹Biogeochemical Integration Department, Max Planck Institute for Biogeochemistry, Jena, Germany

²International Max Planck Research School (IMPRS) for Global Biogeochemical Cycles, Jena, Germany

³Michael Stifel Center Jena for Data-driven and Simulation Science, Jena, Germany

⁴Computational Science Laboratory, Microsoft Research Cambridge, Cambridge, UK

Correspondence to: Johannes Meyerholt (jmeyer@bgc-jena.mpg.de)

Received: 23 November 2015 – Published in Biogeosciences Discuss.: 9 December 2015

Revised: 25 February 2016 – Accepted: 26 February 2016 – Published: 10 March 2016

Abstract. Including a terrestrial nitrogen (N) cycle in Earth system models has led to substantial attenuation of predicted biosphere–climate feedbacks. However, the magnitude of this attenuation remains uncertain. A particularly important but highly uncertain process is biological nitrogen fixation (BNF), which is the largest natural input of N to land ecosystems globally. In order to quantify this uncertainty and estimate likely effects on terrestrial biosphere dynamics, we applied six alternative formulations of BNF spanning the range of process formulations in current state-of-the-art biosphere models within a common framework, the O-CN model: a global map of static BNF rates, two empirical relationships between BNF and other ecosystem variables (net primary productivity and evapotranspiration), two process-oriented formulations based on plant N status, and an optimality-based approach. We examined the resulting differences in model predictions under ambient and elevated atmospheric [CO₂] and found that the predicted global BNF rates and their spatial distribution for contemporary conditions were broadly comparable, ranging from 108 to 148 Tg N yr⁻¹ (median: 128 Tg N yr⁻¹), despite distinct regional patterns associated with the assumptions of each approach. Notwithstanding, model responses in BNF rates to elevated levels of atmospheric [CO₂] (+200 ppm) ranged between -4 Tg N yr⁻¹ (-3 %) and 56 Tg N yr⁻¹ (+42 %) (median: 7 Tg N yr⁻¹ (+8 %)). As a consequence, future projections of global ecosystem carbon (C) storage (+281 to +353 Pg C, or +13 to +16 %) as well as N₂O emission (-1.6

to +0.5 Tg N yr⁻¹, or -19 to +7 %) differed significantly across the different model formulations. Our results emphasize the importance of better understanding the nature and magnitude of BNF responses to change-induced perturbations, particularly through new empirical perturbation experiments and improved model representation.

1 Introduction

Understanding the mechanisms underpinning feedbacks between climate change and land carbon (C) storage is a major challenge in Earth system research (Friedlingstein et al., 2006; Bonan, 2008; Arora et al., 2013; Smith et al., 2013). Ecosystem nitrogen (N) availability strongly affects terrestrial vegetation and soil responses to climate change (Hungate et al., 2003; Gruber and Galloway, 2008; Zaehle, 2013). The terrestrial N cycle receives inputs from atmospheric deposition and biological N fixation (BNF) and ecosystem outputs as leaching and gaseous losses, which together determine the long-term terrestrial N balance and thus N availability. Statistical studies have suggested that the contemporary magnitude and likely future changes in BNF may be an important factor in regulating the amount of N available to support future ecosystem C sequestration, particularly in response to elevated atmospheric carbon dioxide (CO₂) concentrations (*e*CO₂) (Hungate et al., 2003; Wang and Houlton, 2009); however, these suggestions were made without pro-

viding detailed knowledge on the underlying spatio-temporal development of BNF and its driving factors.

A new generation of terrestrial biosphere models (TBMs) that include a representation of the dynamics of various N cycle components has been developed to analyse the consequences of limited terrestrial N availability; see Zaehle and Dalmonech (2011) for a review. These C–N models predict that ecosystem N availability attenuates the responses of the terrestrial C cycle to $e\text{CO}_2$ and climate change, thereby altering the C-cycle-related biosphere–climate feedbacks (Thornton et al., 2007; Sokolov et al., 2008; Zaehle et al., 2010b; Arora et al., 2013; Smith et al., 2014; Zhang et al., 2014). Furthermore, atmospheric CO_2 and climate change modulate the terrestrial source of the greenhouse gas N_2O , potentially providing an additional feedback to the climate system (Stocker et al., 2013; Zaehle, 2013). However, many aspects of the functioning of the terrestrial N cycle and its interactions with the C cycle, as well as the causes of widespread terrestrial N limitation, remain poorly understood.

One reason for the occurrence of N limitation is that BNF, the microbial reduction of quasi-inert atmospheric N (N_2) to plant-available reactive N, is an energy-costly process and therefore not ubiquitous in many energy-limited ecosystems (Postgate, 1970; Vitousek and Howarth, 1991). Symbiotic BNF is carried out by microbes that inhabit root nodules in plants (Gutschick, 1981) and is commonly assumed to contribute the bulk of global BNF (Cleveland et al., 1999). Plants that exhibit these symbioses with microbes, often legumes, are frequently referred to as “N fixers”. Asymbiotic forms of BNF include plant-associated BNF (N-fixing microbes inhabiting the plant rhizosphere but not entering direct plant–microbe symbioses), as well as heterotrophic BNF carried out by free-living bacteria. Furthermore, BNF from mycorrhizal fungi (Franklin et al., 2014) and cryptogamic communities (Elbert et al., 2012) has been shown to be of significant magnitude. These groups of N fixing organisms are phylogenetically diverse and poorly understood (Vitousek et al., 2013), making the quantification of global BNF rates challenging. Efforts towards global-scale quantifications of ecosystem BNF rates have not progressed beyond integrated biome-scale estimates extrapolated from few point measurements ($100\text{--}290\text{ Tg N yr}^{-1}$; Cleveland et al., 1999) and estimates based on heuristic assumptions (128 Tg N yr^{-1} ; Galloway et al., 2004; $44\text{ or }58\text{ Tg N yr}^{-1}$, Vitousek et al., 2013). Such understanding has been hampered by practical and methodological uncertainties in plot-scale measurements, as well as by regional undersampling.

Although these rates indicate that BNF is the largest natural input of reactive N to the terrestrial biosphere and N fixing plants should have a competitive advantage in N-limited ecosystems such as old-growth temperate and boreal forests, the N input from BNF is not sufficient to lift the widespread N limitation of terrestrial production (Vitousek and Howarth, 1991). Rather, symbiotic BNF in particular has been characterized as an early successional phenomenon. The absence

of N fixers from high-latitude old-growth forests has been attributed to co-limitation by the availability of other resources (most prominently phosphorus and/or light, both of which are required in higher abundance by N fixers relative to non-fixers), environmental factors such as soil temperature, and increased herbivory preference for N fixers (Vitousek and Field, 1999; Vitousek et al., 2002; Wang et al., 2007; Houlton et al., 2008; Menge et al., 2008). To date, such insights on the controlling factors of BNF have not been incorporated into models meant for global representation of biogeochemical processes in the biosphere.

The majority of C–N TBMs relies on the empirical relationship between observation-based estimates of BNF and actual evapotranspiration (ET) developed by Cleveland et al. (1999), based on earlier works suggesting a link between high rates of BNF and water losses in humid ecosystems (Schimel et al., 1996). This approach was originally taken with the awareness that it largely ignored the biogeochemistry of BNF, and it was thus applied as a (time-invariant) climatology to drive N cycle models (Zaehle et al., 2010b), but also applied as a dynamic-process representation (Yang et al., 2009; Wania et al., 2012; Smith et al., 2014). Cleveland et al. (1999) also presented a second, considerably weaker correlation of BNF with net primary productivity (NPP), which was subsequently applied in TBMs as well (Thornton et al., 2007; Goll et al., 2012).

Other model representations were developed for global models to treat BNF based on plant physiology rather than empirical relationships. Gerber et al. (2010) presented an approach that determines ecosystem BNF rates based on vegetation N demand, availability of soil reactive N, and light availability. In this model, simulated BNF rates are the result of biogeochemical ecosystem processes and also take effects of forest succession or disturbance into account. Another class of models has focused on the optimization of plant C investment into resource acquisition (Rastetter et al., 2001; Wang et al., 2007; Fisher et al., 2010), including symbiotic BNF. Here, ecosystem BNF rates are the result of a cost–benefit evaluation that maximizes the plants’ competitiveness for nutrients. This concept was subsequently applied to generate symbiotic BNF input rates for a TBM as well (Wang et al., 2010).

It is presently unclear how the uncertainty regarding terrestrial BNF affects the projections of terrestrial biosphere dynamics. In a first attempt, Wieder et al. (2015) tested the BNF representations based on empirical BNF to NPP and ET relationships as described by Cleveland et al. (1999) in the Community Land Model, version 4.5 (CLM4.5) under the “business-as-usual” representative concentration pathway (RCP) 8.5 (Moss et al., 2010). They found a moderate global BNF increase for the NPP approach and an eventual BNF decrease for the ET approach. While informative, this study only considered the two most common BNF representations, both of which are simple enough for their responses to global change and the consequences for model predictions

to be relatively straightforward. Other approaches, however, might introduce more complexity into the simulated biosphere responses to change, which calls for a comparison of a more complete set of BNF representations in TBMs.

To assess this uncertainty, we tested six alternative approaches to represent BNF embedded within the framework of a common TBM, the O-CN model (Zaehle and Friend, 2010), which comprises a comprehensive description of the terrestrial C and N cycles and their interactions with the terrestrial energy and water balance. Applying all BNF schemes directly in a full TBM allowed us to appraise the consequences of uncertainty in BNF representations for the simulated C cycle. The BNF models included a prescribed global map of static BNF rates, two simple empirical relationships between BNF and other ecosystem variables (NPP and ET), two formulations based on plant N status, and an approach following a basic form of optimality of plant N acquisition (Table 1).

We first applied these alternative BNF model versions of O-CN to simulate the pre-industrial to present-day global patterns of the terrestrial C and N cycle to analyse the implied spatial patterns of BNF and associated projected C and N fluxes. We then sought to test the implied sensitivity of BNF, and thus the coupled C–N cycles, to changes in N limitation. We did this by driving the model versions with idealized transient and stepwise $e\text{CO}_2$ scenarios to make the functional model differences clearly apparent. The increased C availability increased plant N demand, and this demand was met with a variety of approaches to determine the ecosystem N input of BNF, which emphasized the different characteristics of the alternative approaches. In particular, we expected a pronounced discrepancy between empirical and mechanistic BNF representations, highlighting a previously unquantified source of variation in the predictions of C–N terrestrial biosphere models.

2 Methods

2.1 O-CN

The O-CN model (Zaehle and Friend, 2010) is an extended version of ORganizing Carbon and Hydrology in Dynamic Ecosystems (ORCHIDEE) (Krinner et al., 2005), the land surface model of the Institut Pierre Simon Laplace (IPSL) Earth system model (Dufresne et al., 2013). O-CN has been extended to represent, among other things, key terrestrial N cycle processes in the vegetation and soil compartments (Fig. 1). It simulates density-based representations of the C and N dynamics of 12 plant functional types (PFTs) on a global grid, and is applied here at a spatial resolution of $1^\circ \times 1^\circ$. The representation of the N cycle includes (1) prognostic plant tissue and soil organic matter N concentrations; (2) N-dependent leaf-level photosynthesis and plant respiration; (3) N-dependent allocation of assimilates to various

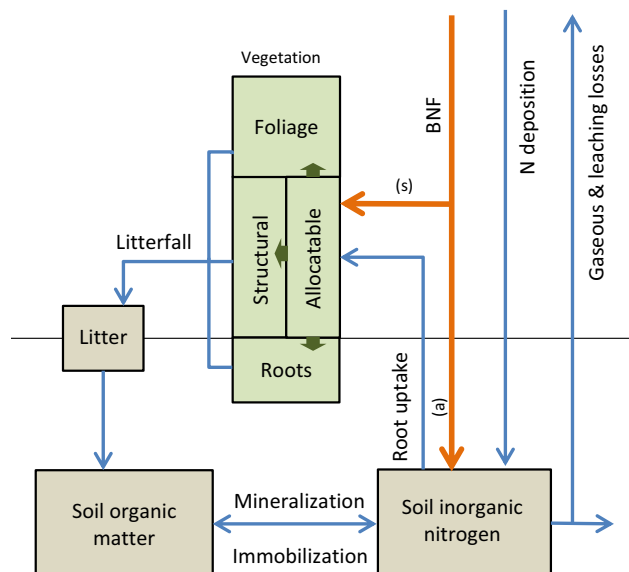


Figure 1. Scheme of nitrogen (N) cycle representation in O-CN. Reactive N species (ammonium, nitrate) enter the ecosystem through atmospheric deposition directly into the pool of soil inorganic N, as well as through biological N fixation (BNF, as ammonium). N from asymbiotic BNF (a) enters the soil inorganic N pool, whereas N from symbiotic BNF (s) becomes directly available to plants for allocation to their various organs. N in plant litter is assimilated into soil organic matter and may be mineralized and transferred to the soil inorganic N pool, depending on that pool's size and the C:N ratio of the soil organic matter. The soil inorganic N pool is depleted by plant root N uptake, and immobilization (transfer to soil organic matter), as well as by leaching or gaseous loss processes. Global magnitudes of the key N fluxes in O-CN can be found in Table 2. O-CN does not include fluxes of geological N inputs, plant organic N uptake, or canopy N uptake.

plant organs with different C:N ratios; (4) N-dependent soil organic matter decomposition and N mineralization, following the CENTURY soil model (Parton et al., 1993); (5) N inputs from atmospheric deposition and fixation, as well as leaching and gaseous N losses resulting from nitrification and denitrification processes in the soil. The treatment of inorganic soil N (Zaehle et al., 2011) largely follows the Lund–Potsdam–Jena Dynamic Nitrogen scheme (LPJ-DyN) approach (Xu and Prentice, 2008), with additions from the DeNitrification and DeComposition (DNDC) model (Li et al., 2000). See Zaehle and Friend (2010) for a detailed description of O-CN.

2.2 BNF models

We conducted simulations applying six alternative models of symbiotic BNF currently applied in TBMs, which are described in Sects. 2.2.1 to 2.2.6 (Zaehle and Dalmonech, 2011; Table 1; Appendix A). Conceptually, the BNF models can be summarized as model forcing (time-invariant map of BNF

Table 1. Overview of the different biological nitrogen (N) fixation (BNF) models used in this study. Appendix A provides full details of the models. NPP: net primary productivity; ET: actual evapotranspiration (excluding soil evaporation); *T*: air temperature.

BNF model	FOR	AET	PRO	NDT	NDS	OPT
Type	Forcing		Empirical		N-demand based	Optimal
Asymbiotic BNF	Global map of BNF rates, based on correlation with ET; BNF		$f(\text{soil temperature, shading, soil moisture})$			
Symbiotic BNF	converges towards zero when soil N pool exceeds 2 g N m^{-2}	$f(\text{ET})$	$f(\text{NPP})$	$f(\text{plant N demand, } T, \text{ plant labile C reserve})$	$f(\text{plant N demand, shading outside tropics, leaf C})$	$f(\text{plant C cost of root N uptake, root C})$
Reference	Zaehle and Friend (2010)	Cleveland et al. (1999)	Thornton et al. (2007)	–	Gerber et al. (2010)	Rastetter et al. (2001)

rates (FOR)); two empirical models relating N fixation to vegetation production or water loss, as presented by the review of Cleveland et al. (1999) (AET, PRO); two process-oriented models that heuristically account for the dependency of N fixation on vegetation N demand (NDT, NDS); and one model following a basic concept of plant fitness optimality of N acquisition (OPT). As only the FOR model implicitly accounted for asymbiotic N fixation, the other five models included an additional term representing this pathway that contributes strongly to N fixation in ecosystems with low vegetation cover (derived in Sect. 2.2.7). N fixed through symbiotic BNF was added to the labile N pool of the plants, whereas asymbiotic BNF was added to the ammonium soil pool.

2.2.1 FOR

The FOR model uses a static global map of BNF rates as model forcing, derived from an empirical, linear correlation between data-based estimates of ecosystem BNF rates and modelled ET (Cleveland et al., 1999). The map was derived by using Cleveland's central regression parameters with a climatology of 1961–2000 ET (Prentice et al., 1993). To avoid N accumulation in systems with low plant N requirement (i.e. low plant productivity or high N availability), BNF in this approach is set to converge towards zero when soil inorganic N concentrations exceed 2 g N m^{-2} . Thus, average BNF rates still vary due to any mechanics that affect the soil N pool, such as seasonal variations in plant N uptake and organic-matter mineralization, or long-term shifts in these quantities under perturbation. Because this approach does not separate between symbiotic and asymbiotic pathways, BNF in FOR is added directly to the soil N pool. This is the original O-CN BNF representation (Zaehle and Friend, 2010).

2.2.2 AET

The AET model determines BNF as a linear function of modelled ET, based on the observation that high BNF rates occur

in humid ecosystems that have large N stocks, but also high N loss rates (Schimel et al., 1996). The most widely used parametrization for this regression is the central estimate of the slope between ET and BNF, as estimated by Cleveland et al. (1999), which is also applied here. The difference between the FOR and AET models is that in FOR, ET is the time-invariant annual evapotranspiration, whereas in AET, ET is the daily evapotranspiration as prognostically modelled by the water and energy flux component of O-CN (Krinner et al., 2005). This BNF representation was previously applied in the Integrated Science Assessment Model (ISAM; Yang et al., 2009), University of Victoria (UVic; Wania et al., 2012), and Lund–Potsdam–Jena General Ecosystem Simulator (LPJ-GUESS; Smith et al., 2014) models.

2.2.3 PRO

The PRO model determines BNF as a function of the daily modelled NPP. The model is based on the estimates presented in Cleveland et al. (1999) and follows the qualitative observation (Vitousek and Howarth, 1991) that the highest BNF rates are typically observed in high-productivity ecosystems. Instantaneous BNF is calculated as a saturating function of NPP, ensuring that the fixation rate does not increase strongly when NPP is high. This BNF representation was previously used in the CLM (Thornton et al., 2007) and Jena Scheme for Biosphere–Atmosphere Coupling in Hamburg (JSBACH; Goll et al., 2012) models.

2.2.4 NDT

The NDT model considers BNF as a supplementary pathway to N uptake via roots, allowing both uptake pathways to co-occur in time and space. BNF is assumed to be primarily driven by the difference between the ability of plants to acquire N from the soil and their N demand according to their C assimilation. Thus, BNF increases linearly with foliar C : N above a PFT-specific value, related to the PFT-specific average observed foliar C : N. The energy cost required for fixing

N is assumed to be satisfied by the available labile C reserve and is assumed to follow an inverse bell-shaped function of daily temperature due to the kinetics of the nitrogenase enzyme (Houlton et al., 2008). Thereby, the assumption is made that in environments colder (or warmer) than 25 °C, more C needs to be invested into BNF (Fisher et al., 2010). The costs of root N uptake are implicitly accounted for through root turnover, leading to higher uptake costs for higher investment into uptake structures (i.e. roots) to attain a given rate of BNF. BNF is thus limited by the N status of the plant and its C resources.

2.2.5 NDS

The NDS model is driven by plant N demand and follows the BNF representation in the LM3V model (Gerber et al., 2010). The model up- and down-regulates BNF rates as a function of the plants' N requirement and N status, as well as light limitation outside the tropics. From potential NPP, the amount of N required to support this growth is determined according to the current plant tissue C : N and allocation fractions. The plant's N deficit is then determined as the difference to the N available in the labile N pool, which contains the N from root uptake. The plants' N status is taken into account to ensure that BNF increases when plants are more N-limited, determined by the relationship between current leaf C : N and prescribed maximum and minimum ratios.

2.2.6 OPT

The OPT model uses an optimality-based approach that follows the concept described by Rastetter et al. (2001). In this model, BNF only occurs when the C cost of BNF, indicative of energy (glucose) investment, is lower than the C cost of root N uptake. This cost of C investment in root N uptake is evaluated as the potential plant C gain if a marginal amount of C was allocated to leaves for photosynthesis, relative to the potential plant N gain if that same marginal amount of C was allocated to increase fine root mass instead. This way, the C cost of root N uptake is defined as the amount of C from photosynthesis the plant relinquishes in favour of investment into root N uptake. If this cost is higher than the (fixed) C cost of BNF, BNF occurs and is determined as a saturating function of root mass and the difference in C cost between root N uptake and BNF. Notably, the occurrence and magnitude of BNF do not feed back on the determination of plant root N uptake in this approach.

As described by Rastetter et al. (2001), BNF is favoured in OPT when the environmental conditions promote high photosynthetic efficiency, e.g. through high irradiation or elevated atmospheric CO₂ concentrations, and increasing leaf mass is a worthwhile investment. Furthermore, high plant root mass or low soil inorganic N availability will increase the C cost of increasing root N uptake and consequently favour BNF. This approach has not been used in a TBM thus

far. However, a modified version that includes phosphorus dynamics (Wang et al., 2007) was used to generate symbiotic BNF input for the Carnegie–Ames–Stanford approach (CASA; Wang et al., 2010).

2.2.7 Asymbiotic BNF

Asymbiotic BNF was calculated for the fraction of the soil receiving light, thus declining with increasing light interception by the vegetation. A maximum rate of 0.2 g N m⁻² yr⁻¹ was assumed based on the data presented by Cleveland et al. (1999), which was modulated by soil moisture availability and soil temperature to account for reduced biochemical activity in dry, cold, or hot environments.

2.3 Modelling protocol and experiment design

All simulation experiments were repeated for each of the six BNF models described above. The aim was to elucidate the effects of the alternative representations on estimates of present-day BNF and its impact on terrestrial C and N cycles, as well as on projections of the consequences of increasing atmospheric CO₂ concentrations, a key factor in decreasing N availability over time.

Prior to all experiments, the O-CN soil and vegetation C and N pools were spun up to equilibrium for each BNF approach separately under representative pre-industrial forcing, including pre-industrial atmospheric CO₂ concentrations (Etheridge et al., 1996; Sitch et al., 2015), estimated 1860 atmospheric N deposition (Lamarque et al., 2010), estimated 1860 land use from the HYDE database (Goldewijk et al., 2001), PFT distribution from the SYNMAP data set (Jung et al., 2006), estimated 1860 artificial N fertilizer application as described in Zaehle et al. (2011), as well as climate data of randomly drawn years (1901–1930) from the merged product of the Climate Research Unit observed climatology and the National Centers for Environmental Prediction re-analysis (CRU-NCEP; N. Viovy, personal communication, 2014). From the 1860 state, we performed a transient simulation from 1860 to 2013 with time-varying climate, N deposition, land use, and fertilizer data, as well as observed changes in atmospheric CO₂ concentration (A; Fig. 2). We used this simulation to evaluate the differences in estimates of the global C and N cycles under present-day conditions, as described in Sect. 3.1.

We then evaluated the effect of eCO₂ on terrestrial C and N fluxes for the different models by comparing A to a simulation with a larger increase in atmospheric CO₂ concentrations (B; Fig. 2), with the other forcings as in A (Sect. 3.2). To avoid a dependency of the simulations on a specific future emission pathway under a particular scenario, we applied a monotonic increase in atmospheric CO₂ from 1860 conditions (286 ppm) at a rate of 0.5 % yr⁻¹, which corresponds to an average growth rate of 2.1 ppm yr⁻¹, approximately comparable to the currently observed growth rate of atmospheric

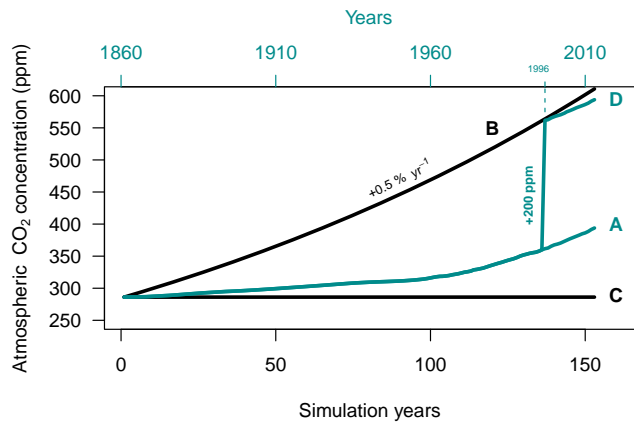


Figure 2. Atmospheric CO₂ concentrations applied in the simulations.

CO₂, arriving at 600 ppm at the end of the simulation. We also compared B to a simulation with CO₂ fixed at 1860 conditions (286 ppm, C) to elucidate the cumulative effect of e CO₂ on the time evolution of key ecosystem fluxes and stocks of C and N.

The BNF models likely have different sensitivities to different timescales of e CO₂ perturbations, which subsequently could feed back on model predictions. Therefore, we further evaluated the effect of timescale by adding a step increase in CO₂ to the transient simulation A. For this experiment (D), atmospheric CO₂ concentrations were increased relative to A by 200 ppm for every year from 1996 (or simulation year 136) onwards. In other words, we simulated a global Free Air CO₂ Enrichment (FACE) experiment, akin to actual local-scale FACE field experiments (McCarthy et al., 2010; Norby et al., 2010). While these experiments are artificial in their step increases in atmospheric CO₂ concentrations, they provide clear insights into direct vegetation responses to e CO₂ (Zaehle et al., 2014). This experiment enabled us to compare the simulated ecosystem responses to e CO₂ between the gradual and step-increase e CO₂ experiments (B vs. C and D vs. A).

3 Results

3.1 Ambient atmospheric CO₂ concentrations

The model-median simulated global BNF rates (simulation A) for the 2000–2013 period (Fig. 3a) followed a distribution that was largely consistent with previous estimates (Cleveland et al., 1999). BNF increased approximately along a latitudinal gradient from arctic and boreal regions (characterized by low surface temperatures, low ET, and strong N limitation) to the tropics (characterized by high temperatures, high humidity, and high N turnover). The predicted total global BNF rates for 2000 ranged from 108 to 148 Tg N yr⁻¹, with a median of 128 Tg N yr⁻¹ (Table 2). The global rates

of asymbiotic BNF were in the range of 1.4–1.6 Tg N yr⁻¹, which, in dependence on the respective simulated symbiotic BNF, resulted in fractions of asymbiotic BNF in total BNF of between 1.0 % (NDS) and 1.4 % (OPT).

Notwithstanding, individual BNF models differed considerably in their predictions in many regions (Fig. 3b). In Europe, the eastern US, eastern Asia, and extratropical South America, the empirical models (AET, PRO) predicted higher BNF rates than the other approaches. In these regions with widespread human activity, fertilizer application and atmospheric N deposition caused high N availability for plants, which either directly reduced BNF (FOR, OPT) or over time diminished the plants' N demand and thereby BNF (NDT, NDS). These mechanisms did not apply in the empirical models. Another important model difference is the large discrepancy in simulated BNF in northern Russia and Canada (Fig. 3b) that mainly stems from very high BNF rates predicted by the N-demand-based models (NDT, NDS). In both approaches, strong N limitation in these regions increased BNF beyond plausible rates (Cleveland et al., 1999), occasionally in excess of 3 g N m⁻² yr⁻¹ in the case of NDS (Fig. 4b). The lack of temperature control on BNF in NDS resulted in notably higher predicted BNF rates in the boreal zone than in NDT, which led to substantial alleviation of N limitation (Figs. B5–B8).

All models simulated the highest cumulative BNF rates for tropical forests and global grasslands (Fig. 4). Nevertheless, the variation in predicted tropical BNF rates was high. Low tropical BNF in PRO was the result of the prescribed saturating function of BNF with NPP. In OPT, tropical BNF was limited by shading under dense canopy and high soil N abundance. All other models predicted higher tropical BNF rates, governed by ET (FOR, AET), high temperatures (implying low costs of BNF combined with moderate N requirements (NDT)), or high foliar biomass, to which potential BNF rates were scaled (NDS). Grasslands and boreal forests contributed strongly to global BNF particularly for NDS because this model simulated a larger production in boreal and tundra vegetation than the other models, resulting from the implicit feedback between BNF and leaf production (Fig. B2). As noted above, the models disagreed on the amount of BNF from crop vegetation, with the empirical approaches (that do not constrain BNF by the plants' N demand) suggesting the largest rates of agricultural BNF (AET, PRO). For models, in which the plant N status was a determining factor of BNF rates (NDT, NDS), N fertilization reduced the crop plants' N demand, resulting in comparatively low BNF rates. Interestingly, although high soil N availability from fertilization leads to lower BNF in the OPT model, it was not strongly reduced, suggesting that N fertilizer application was not sufficient to lift N limitation in all regions of the world.

The model uncertainty in BNF did not cause large uncertainty in the predicted global gross and net primary productivity (GPP and NPP; Table 2). Notably, the inclusion of res-

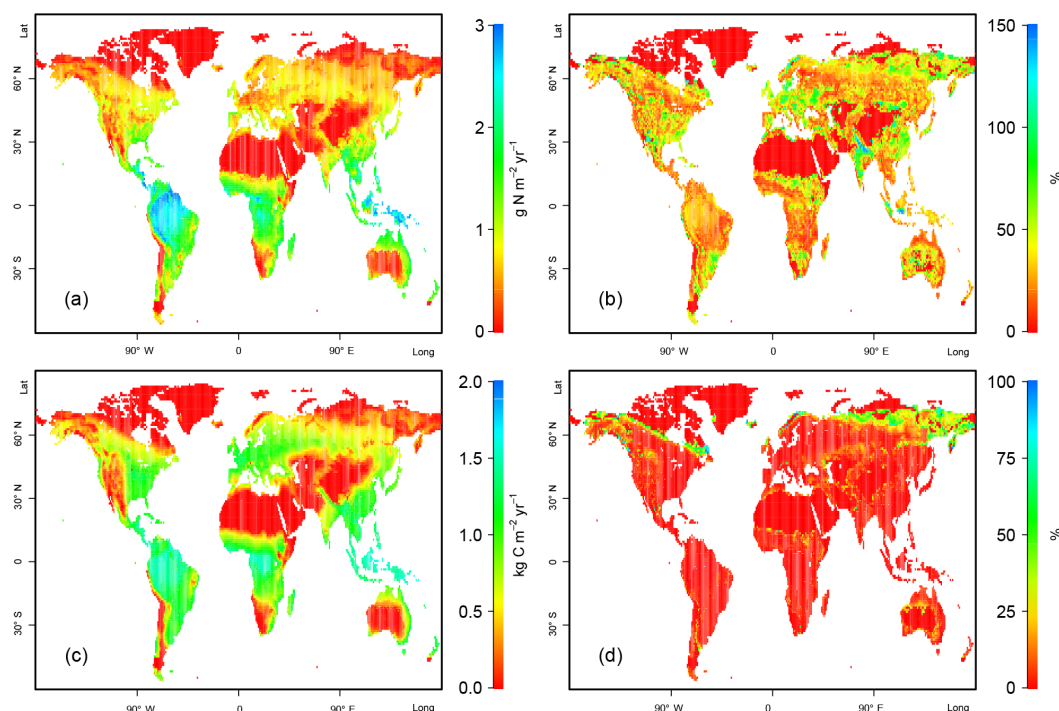


Figure 3. Global biological nitrogen (N) fixation (BNF) and net primary production (NPP) rates, as simulated by O-CN (simulation A) applying the six different BNF models for 2000–2013. Panel (a): model-median BNF ($\text{g N m}^{-2} \text{yr}^{-1}$). Panel (b): median relative deviation (MRD) from the median BNF across models (%). Panel (c): model-median NPP ($\text{kg C m}^{-2} \text{yr}^{-1}$). Panel (d): MRD from the median NPP across models (%). Figures B1 and B2 in the Appendix provide BNF and NPP maps for each model separately.

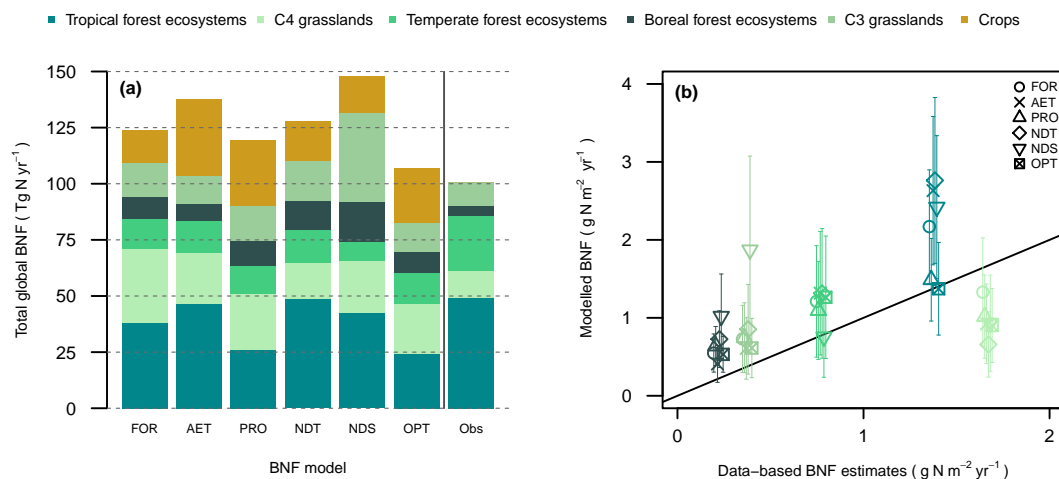


Figure 4. Average biological nitrogen (N) fixation (BNF) rates in different biome types as simulated by O-CN, applying the different BNF models for the year 2000 (simulation A). Panel (a): total global BNF rates (Tg N yr^{-1}); segments indicate the contributions of individual biome types. “Obs” denotes data-based estimates, as published in Table 13 of Cleveland et al. (1999) (conservative estimates of total N fixation). Panel (b): BNF rates ($\text{g N m}^{-2} \text{yr}^{-1}$) as simulated by the different BNF models, compared with the conservative estimates by Cleveland et al. (1999). For the modelled BNF rates, markers indicate the mean value over all grid cells that included the respective biome type; error bars indicate the corresponding standard deviation. The black line is the one-to-one line. Details on the classification of vegetation types from the data source into the plant functional types applied in O-CN can be found in Table B1 in the Appendix.

piration costs of BNF in NDT, NDS, and OPT did not result in a significant reduction in C-use efficiency, potentially because of the reduced severity of N limitation, which reduced

excess respiration. The spatial patterns of simulated rates of NPP were also very similar for large parts of the terrestrial biosphere, despite the diverging rates of BNF (Fig. 3c and

Table 2. Key ecosystem variables as simulated by O-CN applying the different biological nitrogen (N) fixation (BNF) models (global averages for 2000, simulation A). MRD denotes the median relative deviation from the respective model median. For BNF, MRD is taken for the sums of asymbiotic and symbiotic BNF. The same holds for the BNF estimate from FOR, as this model does not distinguish between the two pathways of BNF. “N accumulation” denotes the change in the vegetation and soil N stocks over the year 2000. Our simulations did not include N losses from fire. Note that rounding errors may affect the budget between inputs, losses, and accumulation to a small degree. “Obs” gives literature estimates of global N fluxes where possible.

	MRD	FOR	AET	PRO	NDT	NDS	OPT	Obs
GPP (Pg C yr ⁻¹)	1 %	152	153	153	154	156	149	123–175 ^a
NPP (Pg C yr ⁻¹)	2 %	74	73	75	76	79	76	59.9–62.6 ^b
Plant root N uptake (Tg N yr ⁻¹)	2 %	1349	1250	1275	1281	1338	1267	
N input (Tg N yr ⁻¹)	5 %	272	284	266	274	294	254	
N deposition	–	63	63	63	63	63	63	
N fertilizer	–	83	83	83	83	83	83	
Symbiotic BNF			137	119	127	147	106	
Asymbiotic BNF	10 %	126	1.6	1.5	1.6	1.4	1.5	44–290 ^c
N losses (Tg N yr ⁻¹)	8 %	256	263	246	232	258	228	
N ₂ emission	15 %	90	99	91	86	92	89	
N ₂ O emission	14 %	13	13	12	11	12	10	5–13.8 ^d
NO _x emission	8 %	13	13	12	11	12	11	8.7–11.7 ^d
NH ₃ emission	26 %	5	5	5	3	6	3	31.4–40.4 ^d
Leaching	9 %	108	105	99	92	108	88	59 ^e
Harvest	3 %	27	29	28	29	28	28	
N accumulation (Tg N yr ⁻¹)	34 %	15	20	19	39	33	25	
N loss/mineralization	6 %	0.19	0.19	0.18	0.17	0.18	0.17	
N loss/accumulation	37 %	17	13	13	6	8	9	

^a Beer et al. (2010); Welp et al. (2011). ^b Saugier and Roy (2001). ^c Cleveland et al. (1999); Galloway et al. (2004); Vitousek et al. (2013).

^d Olivier et al. (1998); Ciais et al. (2013). ^e Boyer et al. (2006).

d). This indicated that BNF did not strongly control N limitation throughout regions, and other factors such as light and temperature were also important controls on NPP. Notable exceptions were regions of low production, such as arid and cold regions. The model divergence in NPP in cold regions reflected that the models predicted a variable spread of vegetation growth in the boreal zone. The lower bound of the production range was associated with AET, which simulated very low rates of boreal BNF due to low boreal ET, causing N-limited vegetation growth. On the other hand, the high boreal BNF rates predicted by NDS enabled vegetation growth far into the strongly N-limited tundra regions. In most other regions, especially those with high simulated NPP, the differences between models in BNF barely affected NPP.

The between-model difference in N input rates was, however, reflected in the other branches of the N cycle (Table 2), notably the global terrestrial (including agriculture) gaseous N loss and export of N to groundwater and rivers (subsumed as leaching). The model versions in which BNF was dependent on the N demand of plants (NDT, NDS, OPT) had comparatively low rates of N lost from the ecosystem, likely resulting from the synchronization of ecosystem N input and plant N demand. The variation in N cycle openness (N loss per N mineralization) was low (6 % median relative deviation (MRD)). However, the ratio of N loss to ecosystem N ac-

cumulation was notably lower in the N-demand-based models (37 % MRD) because they predicted both relatively lower losses and relatively higher accumulation. The uncertainty in the magnitude of contemporary emissions of the greenhouse gas N₂O (10–13 Tg N yr⁻¹; 14 % MRD) was close to the uncertainty in BNF (108–148 Tg N yr⁻¹; 10 % MRD).

3.2 Ecosystem responses to eCO₂

We next analysed the effect of increasing N stress through CO₂ fertilization by comparing the final 13 years of the simulations B and A (Fig. 5). For an average atmospheric CO₂ concentration difference of 211 ppm, the predicted total global BNF response to eCO₂ ranged between a 4 Tg N yr⁻¹ reduction (AET) and an increase of 56 Tg N yr⁻¹ (NDS) (median increase of 7 Tg N yr⁻¹), corresponding to –4 and 38 % (median: 6 %) of the average BNF rates under ambient CO₂ (Fig. 3a), respectively. The median predicted responses of global BNF rates to eCO₂ (Fig. 5a and b) indicated a substantial increase in N fixation in many regions. In the N-demand-based approaches, increased C availability increased global plant N demand, having a strong relative effect in boreal and northern temperate regions that were already strongly N limited (Figs. 5b and B3). The eCO₂ experiment also resulted in predicted global NPP increases (Fig. 5c and d). The predictions ranged between 15 and 21 Pg C yr⁻¹ (median:

17 Pg C yr⁻¹), with all models simulating the highest NPP increases in the tropics (Fig. B4).

The increase in BNF rates in responses to *e*CO₂ was by far strongest in the N-demand-based models (Fig. 6). The increased C fixation under *e*CO₂ temporarily increased the simulated labile reserve of allocatable C, which in NDT was directly connected to predicted BNF rates. In NDS, the increase in vegetation N demand outweighed light limitation as a determining factor of BNF responses outside the tropics (Fig. 6a and b). The empirical approaches predicted low (PRO) or negative (AET) global BNF responses (Figs. 6 and B3). The positive effect in PRO was an indirect effect of CO₂ fertilization, whereas the negative effect in AET was driven by the reduction in stomatal conductance in response to *e*CO₂. In OPT, *e*CO₂ led to more efficient photosynthesis, which reduced C allocation to roots for N uptake and thereby increased global BNF rates moderately.

The above variation between models in BNF response magnitudes did not translate into strong disagreement in predicted NPP responses (Fig. 6), as BNF dynamics were not the sole determinant of NPP responses to *e*CO₂. Despite the considerable spread of vegetation into the boreal zone predicted by the N-demand-based models, the largest disagreement was found in the temperate zone (Figs. 6b and B4).

When comparing simulations B and C, the long-term responses to *e*CO₂ in BNF and NPP also affected the global terrestrial C storage and gaseous N emissions (Fig. 7). After 154 years of *e*CO₂ perturbation, the total global ecosystem N stock had increased within a range of 5.1 and 11.9 Pg N. These responses were in part shaped by additional BNF inputs between -0.2 and 11.4 Pg N. The additional ecosystem N supported a total ecosystem C sequestration between 419 and 528 Pg C (Fig. 7c), with the models that predicted high N accumulation per N loss (NDT, NDS, OPT; see Table 2) also predicting high C sequestration. These ecosystem C storage responses correspond to a range of C-concentration interactions in the sense of Gregory et al. (2009) between 1.3 and 1.6 Pg C ppm⁻¹ CO₂, noting that the absolute numbers derived from these studies are not comparable because the increment of gradual CO₂ increase in our study was only half that in Gregory et al. (2009).

The choice of BNF model also had substantial effects on other quantities relevant for biogeochemistry-climate effects, in particular the predicted responses of N₂O emissions to *e*CO₂ (Fig. 7d). In the larger group of models suggesting moderate changes in global and regional BNF, global N₂O emission rates were simulated to decrease with *e*CO₂. With increased C availability, the plants' N demand for constructing new tissue increased as well, depleting the soil N pools and leaving less N for denitrification. However, when the BNF responses became larger over time in NDT and NDS, the BNF increase eventually caused N₂O emission to rise, as larger amounts of N entered the system and became subject to denitrification.

Comparing these long-term *e*CO₂ effects to the effects of a step increase in atmospheric CO₂ concentrations (i.e. comparing simulations D and A) sheds further light on the temporal behaviour of the different BNF models (markers in Fig. 7). The ranking of the BNF schemes in terms of *e*CO₂ response magnitudes was similar between the short-term and long-term experiments. The step increase in atmospheric CO₂ led to short-term BNF responses that were virtually identical to the long-term responses at comparable increases in atmospheric CO₂ concentrations (200 ppm; Fig. 7a). This indicates that the mechanisms shaping *e*CO₂ responses in the different BNF models were already effective in the short-term (less than 5 simulation years). Uncertainty in the short-term BNF response led to a range of global NPP stimulation between 20 and 30 % for the 200 ppm increase. However, the NPP responses in the short-term experiments were systematically lower than in the scenario with gradually increased atmospheric CO₂ (Fig. 7b), indicating the importance of ecosystem N accumulation through enhanced BNF for determining the CO₂ response of plant production in the long-term experiments. None of the models predicted a quick increase in N₂O emission, as this was a soil N accumulation effect over time (Fig. 7d). However, the variability between BNF models was already sizable and qualitatively similar to the long-term experiment, with the N-demand-based models resulting in the smallest decrease in N₂O emission in response to *e*CO₂.

4 Discussion

Given the large variation in approaches used to calculate BNF in this study, ranging from empirical correlation to process-oriented models, our simulations resulted in surprisingly similar estimates of BNF for the contemporary period over large parts of the terrestrial biosphere, despite very notable regional differences. The predicted range of global present-day BNF rates of 108–148 Tg N yr⁻¹ compared reasonably well with the conservative end of the data-based estimates of 100–290 Tg N yr⁻¹ (Cleveland et al., 1999), which had been used to inform the central estimate of 128 Tg N yr⁻¹ in Galloway et al. (2004). Furthermore, the estimates compare well with the higher end of the more recent, inverse estimate of 40–100 Tg N yr⁻¹ (Vitousek et al., 2013), referring to pre-industrial BNF.

One of the prominent regions for which simulated BNF was highly uncertain were high-latitude ecosystems (Fig. 3). Open vegetation in these ecosystems contributed to very high BNF in the NDS scheme in boreal forests and grasslands (Fig. 4b), which made this scheme distinct from the others in this region. We also found a strong heterogeneity of predicted BNF rates for tropical forests, with the OPT model simulating comparatively low BNF, comparable only to the PRO scheme, which had low tropical BNF resulting from the saturating relationship between NPP and BNF. The other

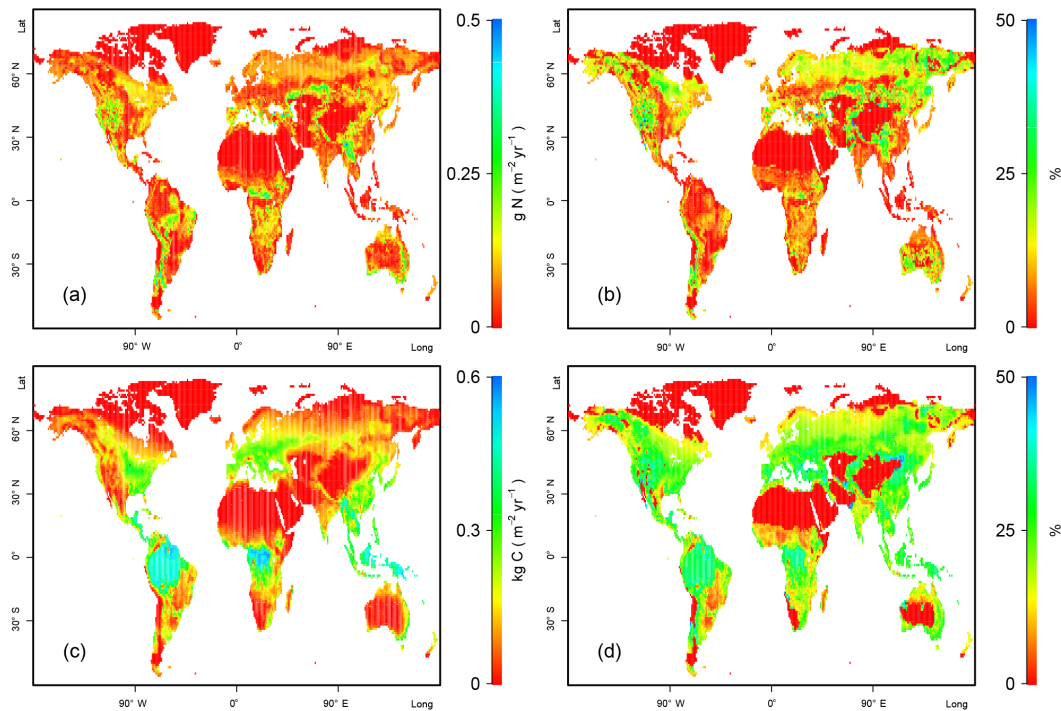


Figure 5. Responses in simulated biological nitrogen (N) fixation (BNF) and net primary production (NPP) rates to elevated atmospheric CO_2 concentrations ($e\text{CO}_2$), taken as the difference between the simulations B ($e\text{CO}_2$) and A (ambient CO_2), averaged over the experiment years 140–153, corresponding to a difference in atmospheric CO_2 concentrations of 211 ppm. Panel (a): absolute model-median BNF responses. Panel (b): relative model-median BNF responses ($(\text{treatment}/\text{control}-1) \times 100, \%$). Panel (c): absolute model-median NPP responses. Panel (d): relative model-median NPP responses. Figures B3 and B4 provide BNF and NPP maps for each model separately.

models tended to simulate substantially higher BNF, either because of high ET (AET), favourable growth conditions and sufficient C supply (NDT), or high leaf area (NDS). It is challenging to judge the validity of any model based on the comparison of our simulations to Cleveland's database, given the large uncertainty in the BNF measurements themselves, and in particular in the scaling of plant-scale estimates to ecosystem-scale estimates. Nonetheless, even allowing for a high uncertainty range in the data, the large predicted values of the NDS scheme in the high latitudes appear unlikely. Similarly, the lack of a response of the empirical schemes to N availability caused these schemes to predict likely too high BNF in intensively fertilized croplands due to their presumed static relationship between BNF and AET or NPP (AET, PRO; Figs. 3 and B1), entailing larger N losses simulated by these schemes in croplands. Finally, our simulations suggest high-latitude and tropical ecosystems to be the most important regions to gather new data from in order to reduce uncertainty in the current generation of BNF models.

In order to further elucidate the consequences of the alternative hypotheses about the control of BNF in the current generation of global ecosystem models, and thus to test the suitability of these models for modelling terrestrial biosphere dynamics, we analysed the response of BNF to a perturbation of the N limitation experienced by the vegetation through

manipulation of its C uptake. The consequences of variety in BNF representation were apparent in the modelled global BNF responses to $e\text{CO}_2$ (Figs. 6 and 7a), which included slight decreases, slight to moderate increases, and very large increases. Experimental field studies on BNF under $e\text{CO}_2$ are rare and inconclusive, presumably owing to the regulatory impacts of micronutrients and vegetation dynamics. Field experiments have found very large $e\text{CO}_2$ responses of BNF in fertilized grasslands (Hartwig et al., 2000; Lüscher et al., 2000) but also moderate responses that declined and became negative over time in subtropical oak woodlands (Hungate et al., 2004, 2014). Heterotrophic fixation was shown not to be affected by $e\text{CO}_2$ at the Duke FACE experiment (Hofmockel and Schlesinger, 2007). This calls for further long-term studies that estimate BNF responses to perturbation. The ecosystem-scale controls on BNF are still poorly characterized, and promising hypotheses on the role of forest succession and micronutrients (Vitousek and Howarth, 1991; Houlton et al., 2008) have largely gone untested.

Given the current data availability, we have limited means of evaluating our global model responses for their plausibility. The empirical BNF models FOR, AET, and PRO are based on observed correlations, but they lack the inclusion of process understanding and may thereby lead to counterintuitive model behaviour under perturbation scenarios (Wieder

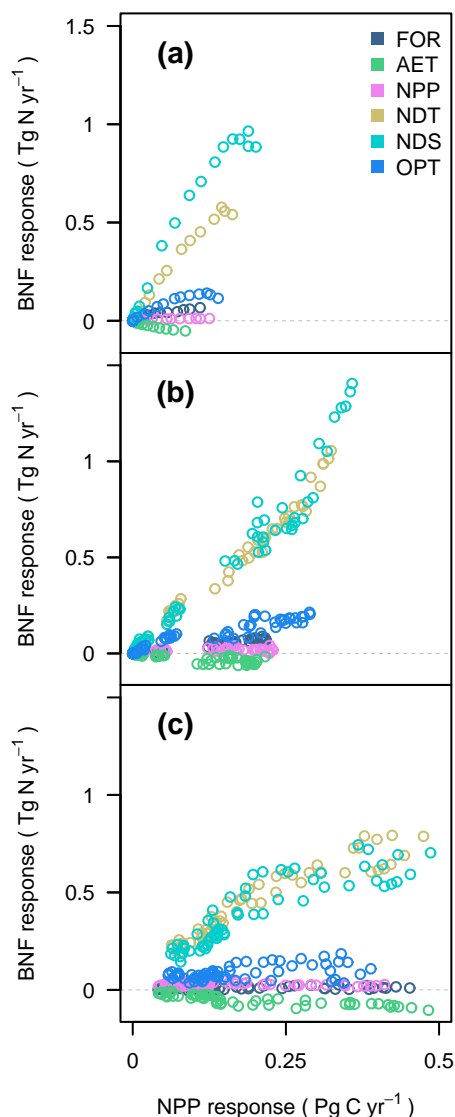


Figure 6. Net primary productivity (NPP) and biological nitrogen (N) fixation (BNF) responses to elevated atmospheric CO₂ concentrations (*e*CO₂), taken as the absolute difference between the simulations B (*e*CO₂) and A (ambient CO₂), averaged over the experiment years 140–153, corresponding to a difference in atmospheric CO₂ concentrations of 211 ppm. Each marker represents one global latitudinal band of 1° extent. Panel (a): responses in the boreal latitudes (90–61° N). Panel (b): responses in the temperate latitudes (60–31° N, 31–60° S). Panel (c): responses in the tropical latitudes (30° N to 30° S).

et al., 2015). In particular, the coupling of BNF with NPP in the PRO scheme can lead to a positive feedback between ecosystem N input and plant growth, which, although attenuated by the saturating nature of the mathematical formulation, remains unsatisfying.

Attempting to incorporate process hypotheses rather than empirical relationships is expedient and also led to lower N losses relative to ecosystem N accumulation in comparison

with other approaches (Table 2), which heuristically appears to be more plausible. Nevertheless, the behaviour of the plant N-status-based models NDT and NDS was likely implausible in other aspects, particularly the strong, quasi-instantaneous increase in BNF under the scenario of a step increase in atmospheric CO₂ (Fig. 7). Short-term BNF responses of such magnitude would have likely been detected in local field experiments, which was not consistently the case (see above). In their current state, NDT and NDS are very sensitive to instantaneous shifts in plant N demand. It was suggested before that, without perturbation, the degree of modelled N limitation is controlled by the magnitudes of BNF and N losses (Thomas et al., 2015). We did not generally find that NDT and NDS predicted higher BNF than other approaches in regions with high N losses. However, the large N inputs under *e*CO₂ resulted in large N losses because more N was added from BNF than could be incorporated into biomass according to vegetation C : N stoichiometry. Also, the fixed N that was used to satisfy the plants' N demand eventually entered the soil through ecosystem turnover, where it became subjected to the N loss pathways. Another key factor for the high BNF responses in NDT and NDS might be the assumption that all types of vegetation are associated with BNF; thus, N-demand-based schemes may benefit from a more explicit distinction between N fixers and non-fixers in the future.

The optimality-based BNF approach described by Rastetter et al. (2001) has thus far not been applied in a TBM, although it was used to generate a static map of BNF inputs for the CASA model (Wang et al., 2010). We have demonstrated here that this approach can be successfully integrated into the dynamic calculations of a global model without any problems of stability or increased computational demand. OPT predicted the lowest amount of global BNF for 2000 (108 Tg N yr⁻¹), which conformed with the recent trend in the literature to postulate lower tropical BNF rates than previously assumed (Sullivan et al., 2014). Optimality has been an emerging perspective in vegetation modelling in recent years, in particular as a means to model plant allocation responses to perturbations such as *e*CO₂ (Dybzinski et al., 2015). For BNF, it does indeed appear reasonable to assume plant BNF activity to be governed by energetic constraints and optimal C investment rather than by a mass-balancing approach. However, one might debate the validity of OPT, as it optimizes C investment into plant N acquisition within the O-CN model that determined all other ecosystem fluxes based on traditional process formulations. Still, OPT could be considered an early example of how optimality could be adapted in TBMs and could be extended to other processes in future model generations. As it stands, however, the lack of global observational constraints prevents a meaningful evaluation of OPT.

Our modelling approach was limited in that it tested BNF formulations within the same O-CN framework that were in part extracted from other TBMs. This entails possible biases in C–N cycle processes other than BNF that are treated dis-

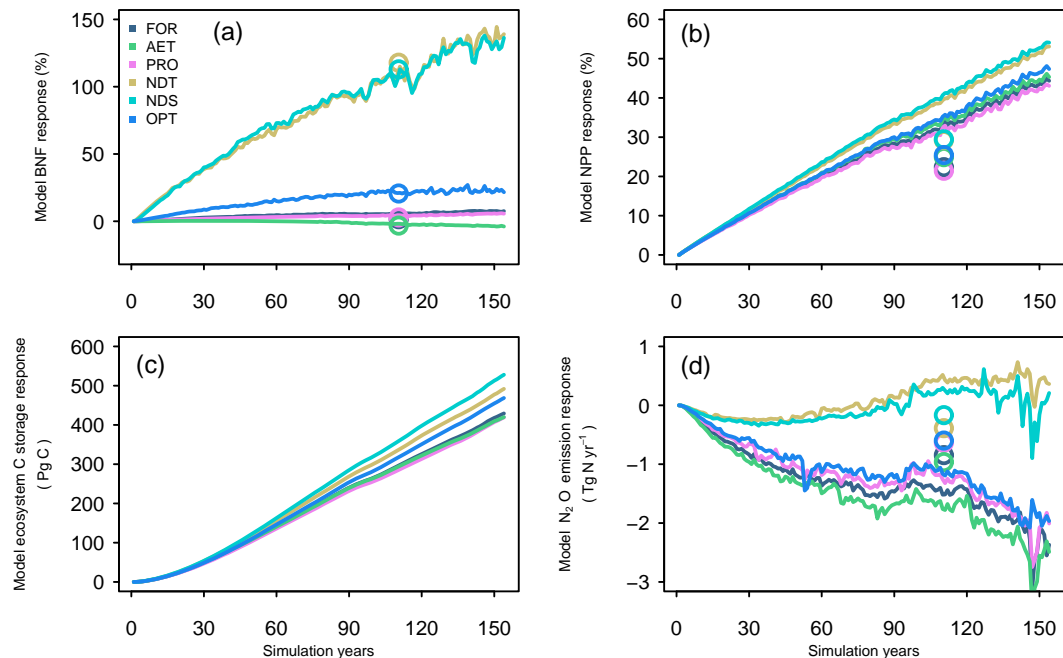


Figure 7. Simulated ecosystem responses to elevated atmospheric CO_2 concentrations ($e\text{CO}_2$) as global time series, obtained using six different biological nitrogen (N) fixation (BNF) schemes. Curves show the differences between the simulations B (atmospheric CO_2 concentrations gradually increasing from 286 to 600 ppm) and C (atmospheric CO_2 fixed at 286 ppm). Markers show the responses between the simulations D (observed atmospheric $\text{CO}_2 + 200$ ppm) and A (observed atmospheric CO_2), calculated as averages over the simulation years 136–140. They are plotted at the simulation year 108, so that for all responses, the difference between control and treatment in atmospheric CO_2 concentration was approximately 200 ppm. Panel (a): relative BNF responses ($(\text{treatment}/\text{control} - 1) \times 100$). Panel (b): relative net primary production (NPP) responses. Panel (c): absolute ecosystem carbon (C) storage responses (treatment – control). Panel (d): absolute N_2O emission responses.

tinctly in O-CN. This includes the plant allocation of assimilates, stoichiometric flexibility in plant tissues (Zaehle and Friend, 2010; Meyerholt and Zaehle, 2015), as well as the inclusion of labile plant C and N pools, which are instrumental in NDT, NDS, and OPT. In fact, the uncertainty between TBMs in representing other N cycle processes may be comparable to the uncertainty in BNF representations (Zaehle and Dalmonech, 2011). Nevertheless, we believe that our adoptions of the BNF approaches are representative, as we used the original model parametrizations (Appendix). For instance, the strong sensitivity of BNF to $e\text{CO}_2$ in NDS was also found for the LM3V model (Huang and Gerber, 2015). The overarching principles that the BNF models follow were not changed, and we trust that consequences of the predicted BNF rates on model functioning would give similar qualitative results in a different framework. The consequences of different parametrizations are fairly obvious for the FOR, AET, PRO, and NDT schemes, as BNF scales directly with the respective parameters (a and b in Eq. (A1) in the Appendix; c and d in Eq. (A2); C_{fix} in Eq. (A3); and j in Eq. A5). This is less obvious for the NDS and OPT schemes, in which the parameters determine either the relationship between plant N status and N demand (NDS) or the assumed Michaelis–Menten kinetics of BNF (OPT). These param-

eter effects can be understood by conceptually considering the respective components of the NDS and OPT schemes (Fig. B9).

The effect of the alternative BNF process representations was significant also for predictions on other contemporary key N fluxes (Table 2, Fig. 7). In particular, we found a pronounced effect of BNF variation on predicted gaseous N emission, including N_2O . This was not only the case for the contemporary period: our results demonstrate a large divergence in the CO_2 response of global N_2O emissions, which, integrated over time, would notably affect atmospheric N_2O concentrations. Notably, the N-demand-based BNF models predicted BNF increases high enough to result in an increase in N_2O emission after some decades of $e\text{CO}_2$. This result is a direct consequence of the representation of N loss processes in O-CN, which bases the magnitudes of loss fluxes on the size of the simulated soil inorganic N pool (Zaehle and Friend, 2010). This approach is very common among TBMs (Zaehle and Dalmonech, 2011), but an alternative approach such as turnover-based N losses might lead to an attenuated effect of BNF uncertainty on N_2O emission.

With local exceptions, uncertainty in BNF had a small effect on the estimated contemporary global vegetation production (NPP) and C storage (Table 2). To first order, this

can be understood by the comparatively low contribution of BNF to annual N uptake in most ecosystems: in O-CN, as in most other TBMs, BNF only makes up approximately 10 % of plant N acquisition, with the rest being satisfied by root N uptake (Table 2). Variation in BNF will therefore only affect plant growth to a smaller degree. In the case of O-CN, the variable C : N stoichiometry in organic tissues further implies that plant N gain does not directly entail plant growth (assuming other factors to be non-limiting), e.g. because tissue N concentrations may be increased to enable more efficient leaf photosynthesis. The small variation in contemporary NPP is further explained by the fact that despite regional differences in N limitation evidenced by moderate regional differences in foliar stoichiometry, on global average, the simulated vegetation growth was not strongly N limited for any BNF approach after model spin-up (1860). It was previously shown that the frequency distribution and median of simulated leaf C : N ratios in O-CN roughly correspond to observations (Fig. S5 in Zaehle et al., 2010b). The simulated leaf C : N ratios were not close to the prescribed minimal and maximal values (Table A2) and approximately similar between BNF approaches (average global ratios between 30 (AET) and 33 (NDS, OPT)).

Unlike the small effect under contemporary conditions, the uncertainty in predicted BNF rates under $e\text{CO}_2$ had a sizeable effect on the predicted NPP and C sequestration, resulting from the differences in gradual ecosystem N accumulation (Fig. 7). The ecosystem N input from BNF became a crucial factor under increased vegetation N stress, and resulted in a 20 % variation of the C sequestration per unit atmospheric CO_2 increase (the C-concentration interaction sensu Gregory et al., 2009). This magnitude of variation is similar to the difference in the C-concentration interaction between entire C–N TBMs (cf. Thornton et al., 2007; Zaehle et al., 2010a), notwithstanding the limited comparability of the absolute interaction terms due to heterogeneous experimental set-ups between our and the other studies. This finding underlines previous suggestions that understanding global BNF is important to enable better-constrained global change predictions (Thomas et al., 2015).

Previous studies have already suggested the importance of future changes in BNF for estimates of the capacity of the terrestrial biosphere to respond to CO_2 fertilization (Hungate et al., 2003; Wang and Houlton, 2009). However, these studies were based on global or hemispheric means, assigned a posteriori stoichiometric ratios to bulk terrestrial C stocks, ignored important components of the terrestrial N cycle (such as N losses) and any transient dynamics, and – more fundamentally – did not account for any interactions of BNF with the C and N cycles. While our results are consistent with these studies regarding the likely magnitude of the global BNF flux uncertainty and possible consequences for terrestrial C stocks, our study offers a more in-depth insight into the importance of BNF, as it dynamically and in a transient manner accounts for all the major feedback mechanisms as-

sociated with changing BNF. Model–model and model–data intercomparison for contemporary and perturbed simulations have allowed us to isolate regions with high or low confidence in the predicted BNF trends and to identify measurements required to reduce uncertainty. Finally, we have been able to make a first assessment on the consequence of BNF uncertainty for future predictions of N_2O emissions, which have been ignored by the studies mentioned above.

5 Conclusions

We have shown that the current generation of TBMs uses BNF representations that lead to variable ecosystem flux predictions in both ambient and $e\text{CO}_2$ scenarios. The consequences of this variation extend beyond the prediction of BNF rates to predictions of other key properties such as ecosystem C storage and N_2O emissions. Given that estimating the severity of N constraints on C cycle responses to global change is a major challenge for TBMs, this process uncertainty needs to be resolved to enable more reliable model predictions. However, in light of the deficient process understanding and limited observational constraints, finding better ways to capture the largest natural ecosystem input of N in models will be challenging. Future work is needed to build and improve on current process-oriented representations. The most likely avenues will presumably include appropriate TBM representations of plant community structural dynamics and phosphorus cycling (Thomas et al., 2015; Wieder et al., 2015). These undertakings will prove challenging in themselves: most TBMs still rely on more or less static PFT representations of vegetation, and the global phosphorus cycle is even more poorly constrained by quantitative process understanding than the N cycle (Reed et al., 2015). While such additions will add new sources of model variation, we suspect BNF to be an example where appropriate N cycle process representation can benefit from the introduction of additional model complexity. Further, we would advise to include the concept of optimality in future BNF representations, as in our estimation, OPT has performed reasonably in the analysis presented here. Not least, current BNF model representations treat symbiotic BNF negligently if at all. A more explicit inclusion of this pathway and its regulatory characteristics is warranted by the important role it plays in several ecosystems (Cleveland et al., 1999).

We contend that improving the representation of BNF in TBMs will be greatly aided by a future emphasis on field experiments conducted under environmental perturbations and will likely require the inclusion of additional ecological and nutritional constraints.

Appendix A: BNF model description

Table A1. List of variable and parameter names used in the description of the biological N fixation (BNF) models (Appendix A). C: carbon; N: nitrogen; PFT: plant functional type. PFT-specific parameters are given in Table A2.

Variable/parameter	Description	Value, unit
Shared		
BNF	Symbiotic BNF rate	$\text{g N m}^{-2} \text{yr}^{-1}$
SLA	Specific leaf area	$\text{m}^2 \text{g}^{-1} \text{C}$
C_{Leaf}	Plant leaf C pool	g C m^{-2}
$CN_{\text{Leaf, min}}$	Minimum attainable leaf C : N ratio (PFT-specific)	–
$CN_{\text{Leaf, max}}$	Maximum attainable leaf C : N ratio (PFT-specific)	–
CN_{Leaf}	Standard leaf C : N ratio (PFT-specific)	–
$CN_{\text{Leaf, act}}$	Actual leaf C : N ratio	–
AET		
ET	Actual evapotranspiration	mm yr^{-1}
a	Slope of the linear function in Eq. (A1)	$0.00234 \text{ g N mm}^{-1} \text{ m}^{-2}$
b	Intercept of the linear function in Eq. (A1)	$-0.0172 \text{ g N m}^{-2} \text{ yr}^{-1}$
PRO		
NPP	Net primary production	$\text{g C m}^{-2} \text{ yr}^{-1}$
c	Coefficient in Eq. (A2)	$1.8 \text{ g N m}^{-2} \text{ yr}^{-1}$
d	Coefficient in Eq. (A2)	$-0.003 \text{ m}^2 \text{ yr g}^{-1} \text{ C}$
NDT		
tf	Temperature sensitivity function	–
T	Surface temperature	$^{\circ}\text{C}$
f	Coefficient in Eq. (A4)	1.25
g	Coefficient in Eq. (A4)	-3.62
h	Coefficient in Eq. (A4)	$0.27^{\circ}\text{C}^{-1}$
i	Reference temperature in Eq. (A4)	50.3°C
j	Fraction of labile C pool for BNF investment in Eq. (A5)	0.05
C_{inv}	Instantaneously available C for investment into BNF	g C m^{-2}
C_{labile}	Plant labile C pool	g C m^{-2}
ξ	Temperature scaling function	–
η	Function scaling with plant N status	–
C_{fix}	C investment cost per unit N fixed	$6 \text{ g C g}^{-1} \text{ N yr}^{-1}$
NDS		
λ_0	Light-unlimited establishment rate of N fixers (PFT-specific)	yr^{-1}
λ	Light-limited establishment rate of N fixers (PFT-specific)	yr^{-1}
ψ	Plant N demand per unit leaf C	$\text{g N m}^{-2} \text{ g}^{-1} \text{ C}$
D	Plant N deficit	g N m^{-2}
κ	Scaling function	–
NPP_{pot}	Allocatable C after respiration	g C m^{-2}
f_{cost}	Scaling factor	–
N_{avail}	Available N for plant growth	g N m^{-2}
φ	Parameter in Eq. (A13)	3
x	Plant N status function	–
BNF_L	BNF per unit leaf C	$\text{g N m}^{-2} \text{ yr}^{-1}$
σ	Decay rate of N fixers (PFT-specific)	yr^{-1}
OPT		
C_{Root}	Plant root C pool	g C m^{-2}
x	Instantaneous C gain per unit leaf area	$\text{g C m}^{-2} \text{ yr}^{-1}$
GPP	Instantaneous gross primary production	$\text{g C m}^{-2} \text{ yr}^{-1}$
gc	Marginal C gain with C investment into leaves	$\text{g C m}^{-2} \text{ yr}^{-1}$
δC	Infinitesimal amount of C	g C m^{-2}
gn	Marginal N uptake increase with root C investment	$\text{g N m}^{-2} \text{ yr}^{-1}$
N_{up}	Root N uptake	$\text{g N m}^{-2} \text{ yr}^{-1}$
$r_{N_{\text{up}}}$	C cost of root N uptake	$\text{g C g}^{-1} \text{ N}$
r_{Fix}	C cost of N fixation	$9 \text{ g C g}^{-1} \text{ N}$
$v_{\text{max, Fix}}$	Maximum BNF per unit root C in Eq. (A19)	$0.0225 \text{ g N g}^{-1} \text{ C yr}^{-1}$
k_{Fix}	Half-saturation constant in Eq. (A19)	$50 \text{ g C g}^{-1} \text{ N}$
Asymbiotic BNF		
ts	Temperature sensitivity function	–
T_s	Soil temperature	$^{\circ}\text{C}$
m	Coefficient in Eq. (A20)	1.25
n	Coefficient in Eq. (A20)	-3.62
o	Coefficient in Eq. (A20)	$0.27^{\circ}\text{C}^{-1}$
p	Reference temperature in Eq. (A20)	50.3°C
vf	Light limitation function	–
Φ	Soil moisture function	–
σ	Amount of water in the soil	mm m^{-2}
z	Depth of soil water reservoir	2 m
σ_{max}	Maximum soil water content	150 mm m^{-3}
BNF_a	Asymbiotic BNF rate	$\text{g N m}^{-2} \text{ yr}^{-1}$
$BNF_{a, \text{max}}$	Maximum asymbiotic BNF rate	$0.2 \text{ g N m}^{-2} \text{ yr}^{-1}$

This text gives full details about the different biological nitrogen (N) fixation (BNF) schemes applied in the O-CN model, as presented in Sect. 2.2. A full list of variables, parameters, and units can be found in Table A1.

A1 AET (Sect. 2.2.2)

$$\text{BNF} = a \cdot \text{ET} + b, \tag{A1}$$

with slope a and intercept b and actual evapotranspiration ET (mm yr⁻¹).

A2 PRO (Sect. 2.2.3)

$$\text{BNF} = c \cdot (1 - e^{d \cdot \text{NPP}}), \tag{A2}$$

with the heuristically derived coefficients c and d and net primary productivity NPP (g C m⁻² yr⁻¹).

A3 NDT (Sect. 2.2.4)

The BNF rate is a function of the carbon (C) available for energy investment into BNF (C_{inv}), the temperature function tf , and a prescribed BNF C investment cost per unit N fixed (C_{fix}):

$$\text{BNF} = C_{\text{inv}} / \left(\frac{C_{\text{fix}}}{\text{tf}} \right). \tag{A3}$$

The function tf scales with surface temperature and was adapted from Houlton et al. (2008):

$$\text{tf} = f \cdot e^{g+h \cdot T \cdot (1 - \frac{T}{T_r})}, \tag{A4}$$

where T is the surface temperature in °C. The C available for energy investment into BNF (C_{inv}) is defined as a fraction of the plants' labile C reserve (C_{labile}) and modified by two additional functions that represent temperature scaling (ξ) and the dependence on the plants' N concentration (η):

$$C_{\text{inv}} = j \cdot C_{\text{labile}} \cdot \xi \cdot \eta, \tag{A5}$$

where j is the fraction of C_{labile} available for investment into BNF (as C_{labile} also contains the assimilated C available for allocation to plant growth). The ξ function sets C_{inv} to zero at extreme temperatures:

$$\xi = \max \left(1 - \frac{0.1}{\text{tf}}, 0 \right). \tag{A6}$$

The η function scales C_{inv} with the plants' N status, represented by their leaf C : N ratios:

$$\eta = \max \left(\frac{\text{CN}_{\text{Leaf,min}}}{\text{CN}_{\text{Leaf}}} - \frac{\text{CN}_{\text{Leaf,min}}}{\text{CN}_{\text{Leaf,act}}}, 0 \right), \tag{A7}$$

where $\text{CN}_{\text{Leaf,min}}$ is the prescribed minimum leaf C : N ratio, CN_{Leaf} is a prescribed average C : N ratio specific to the respective plant functional type (PFT), and $\text{CN}_{\text{Leaf,act}}$ is the actual instantaneous leaf C : N ratio. When $\text{CN}_{\text{Leaf,act}}$ is lower or equal to CN_{Leaf} , η is zero. Thus BNF only occurs when the leaf N concentrations are below the prescribed optimum.

Table A2. PFT-specific parameters. The CN parameters were used in all models, the λ_0 and σ parameters were used in the NDS model (see Table A1). The PFT classes are defined in Table B1.

PFT	CN _{Leaf}	CN _{Leaf,min}	CN _{Leaf,max}	λ_0 (yr ⁻¹)	σ (yr ⁻¹)
1	25	16	45	12	12
2	25	16	45	12	12
3	35	20	55	1	1
4	42	28	75	0.2	0.2
5	25	16	45	0.2	0.2
6	25	16	45	0.2	0.2
7	42	28	75	0.1	0.1
8	25	16	45	0.1	0.1
9	24	18	36	0.1	0.1
10	26	16	47	1	1
11	26	16	47	1	1
12	35	20	55	1	1

A4 NDS (Sect. 2.2.5)

$$\text{BNF} = \text{BNF}_L \cdot C_{\text{Leaf}}, \tag{A8}$$

where C_{Leaf} is the leaf C pool size and BNF_L is the BNF rate per unit leaf C, described in differential form:

$$\frac{\partial \text{BNF}_L}{\partial t} = \lambda \cdot \psi - \sigma \cdot \text{BNF}_L, \tag{A9}$$

where σ is the PFT-specific timescale associated with the down-regulation of BNF, ψ is the plants' N demand per unit leaf C, and λ is the characteristic timescale of BNF up-regulation, based on the PFT-specific timescale λ_0 . For tropical plants, $\lambda = \lambda_0$. For all other PFTs, the up-regulation of BNF is light-driven and influenced by leaf shading:

$$\lambda = \lambda_0 \cdot e^{-0.5 \cdot \text{SLA} \cdot C_{\text{Leaf}}}, \tag{A10}$$

where SLA is the specific leaf area. The establishment of BNF is controlled by the plants' local N demand ψ per unit leaf C, which in turn is determined by the plant N deficit (D) and a function (κ) that scales the advantageousness of BNF with the plants' N status:

$$\psi = \frac{D \cdot \kappa}{C_{\text{Leaf}}}. \tag{A11}$$

We define D as the difference between the N that is required to build new biomass from newly acquired C and the N that is available to the plant for allocation to new biomass:

$$D = \text{NPP}_{\text{pot}} \cdot \frac{f_{\text{cost}}}{\text{CN}_{\text{Leaf}}} - N_{\text{avail}}, \tag{A12}$$

where NPP_{pot} is the allocatable C after respiration costs are satisfied, f_{cost} is a dimensionless scaling factor that accounts for the allocation of N to plant organs with different N concentrations, CN_{Leaf} is a prescribed leaf C : N ratio as an approximation to the target C : N ratio of newly grown biomass,

and N_{avail} is the N available to the plant for new growth, defined as 0.9 times the size of the plant's labile N reserve. κ is a function representing the hypothesis that BNF is more opportune if the plant's growth is more severely N limited, indicated by the plant N status (x):

$$\kappa = \varphi \cdot \frac{e^{-\varphi \cdot x}}{1 - e^{-\varphi}}, \quad (\text{A13})$$

with the parameter φ . We define the plant's N status x by comparing its actual leaf C:N ratio to the prescribed minimum and maximum values:

$$x = 1 - \frac{(1/\text{CN}_{\text{Leaf,min}}) - (1/\text{CN}_{\text{Leaf,act}})}{(1/\text{CN}_{\text{Leaf,min}}) - (1/\text{CN}_{\text{Leaf,max}})}. \quad (\text{A14})$$

$\text{CN}_{\text{Leaf,min}}$ and $\text{CN}_{\text{Leaf,max}}$ are the PFT-specific minimum and maximum leaf C:N ratios attainable in O-CN, and $\text{CN}_{\text{Leaf,act}}$ is the actual instantaneous leaf C:N ratio. As the plant's actual leaf C:N ratio increases from $\text{CN}_{\text{Leaf,min}}$ to $\text{CN}_{\text{Leaf,max}}$, its N status decreases from 1 to 0.

A5 OPT (Sect. 2.2.6)

To determine the instantaneous C gain per unit leaf area (k), we consider the relationship of gross primary productivity (GPP) and the fraction of absorbed photosynthetically active radiation, which depends on the specific leaf area and leaf mass:

$$k = \frac{\text{GPP}}{1 - e^{-0.5 \cdot \text{SLA} \cdot \text{C}_{\text{Leaf}}}}. \quad (\text{A15})$$

We then derive the marginal C gain with C investment into leaves, g_c , from the difference in k when an infinitesimal amount of leaf C (δC) is added to the vegetation:

$$g_c = k \cdot (e^{-0.5 \cdot \text{SLA} \cdot \text{C}_{\text{Leaf}}} - e^{-0.5 \cdot \text{SLA} \cdot (\text{C}_{\text{Leaf}} + \delta C)}). \quad (\text{A16})$$

In O-CN, the increase in root N uptake (N_{up}) with a small increase in root C (C_{Root}) is linear; therefore, we approximate the marginal increase in N_{up} with C investment into fine roots, g_n , as the instantaneous C_{Root} -specific N uptake:

$$g_n = \frac{N_{\text{up}}}{C_{\text{Root}}}. \quad (\text{A17})$$

We then evaluate the C cost of N uptake $r_{N_{\text{up}}}$ as

$$r_{N_{\text{up}}} = \frac{g_c}{g_n}. \quad (\text{A18})$$

If $r_{N_{\text{up}}}$ is larger than the C cost of BNF (r_{Fix} , assumed constant), BNF is calculated as a saturating function of ($r_{N_{\text{up}}} - r_{\text{Fix}}$) and root mass:

$$\text{BNF} = C_{\text{Root}} \cdot v_{\text{max,Fix}} \cdot \frac{(r_{N_{\text{up}}} - r_{\text{Fix}})}{k_{\text{Fix}} + (r_{N_{\text{up}}} - r_{\text{Fix}})}, \quad (\text{A19})$$

where $v_{\text{max,Fix}}$ is a maximum BNF rate and k_{Fix} is a half-saturation constant. In the case of the C cost of BNF being higher than the cost of root N uptake, no symbiotic BNF occurs.

A6 Asymbiotic BNF (Sect. 2.2.7)

The asymbiotic BNF rate scales with the same temperature function applied in the NDT approach, but rather than the surface temperature, the function involves the soil temperature T_s :

$$ts = m \cdot e^{n + o \cdot T_s \cdot (1 - \frac{T_s}{p})}. \quad (\text{A20})$$

Asymbiotic BNF is only calculated for the fraction of the soil surface receiving solar energy. We consider light limitation by applying the simple shading function vf , causing BNF to converge towards zero with canopy closure:

$$vf = e^{(-0.5 \cdot \text{SLA} \cdot \text{C}_{\text{Leaf}})}, \quad (\text{A21})$$

where SLA is the specific leaf area of the respective PFT and C_{Leaf} is the leaf C pool size. Also, the limiting effect of drought conditions on heterotrophic BNF is taken into account by including the soil moisture function Φ :

$$\Phi = \frac{\sigma}{z \cdot \sigma_{\text{max}}}, \quad (\text{A22})$$

where σ is the current amount of water stored in the soil, z is the total depth of the soil reservoir, and σ_{max} is the amount of water stored in a water-saturated soil column. The asymbiotic BNF rate is then obtained as

$$\text{BNF}_a = \text{BNF}_{a,\text{max}} \cdot ts \cdot vf \cdot \Phi, \quad (\text{A23})$$

where $\text{BNF}_{a,\text{max}}$ is the maximum asymbiotic BNF rate (Cleveland et al., 1999).

Appendix B

Table B1. Adaptation of the vegetation types from the original data assembly (Cleveland et al., 1999; Table 13) into the plant functional types (PFTs) in O-CN (“Obs” in Fig. 4).

PFTs in O-CN	Vegetation types in Cleveland et al. (1999)
1. Tropical broadleaved evergreen	Tropical savannah (50 %), tropical evergreen forest, xeromorphic forest, tropical forested floodplain, wet savannah (50 %)
2. Tropical broadleaved raingreen	Tropical deciduous forest
3. C4 grasses	Tropical savannah (50 %), tropical non-forested floodplain, wet savannah (50 %)
4. Temperate needle-leaved evergreen	Temperate mixed forest (50 %), temperate coniferous forest
5. Temperate broadleaved evergreen	Temperate broadleaved evergreen forest
6. Temperate broadleaved summergreen	Temperate mixed forest (50 %), temperate deciduous forest, temperate forested floodplain, temperate steppe (30 %), Mediterranean shrubland, arid shrublands
7. Boreal needle-leaved evergreen	Boreal forest
8. Boreal broadleaved summergreen	Boreal woodland, moist tundra
9. Boreal needle-leaved summergreen	–
10. C3 grasses	Polar desert or alpine tundra, tall or medium grassland, short grassland, desert, temperate non-forested floodplain, temperate steppe (70 %)
11. C3 crop plants	–
12. C4 crop plants	–

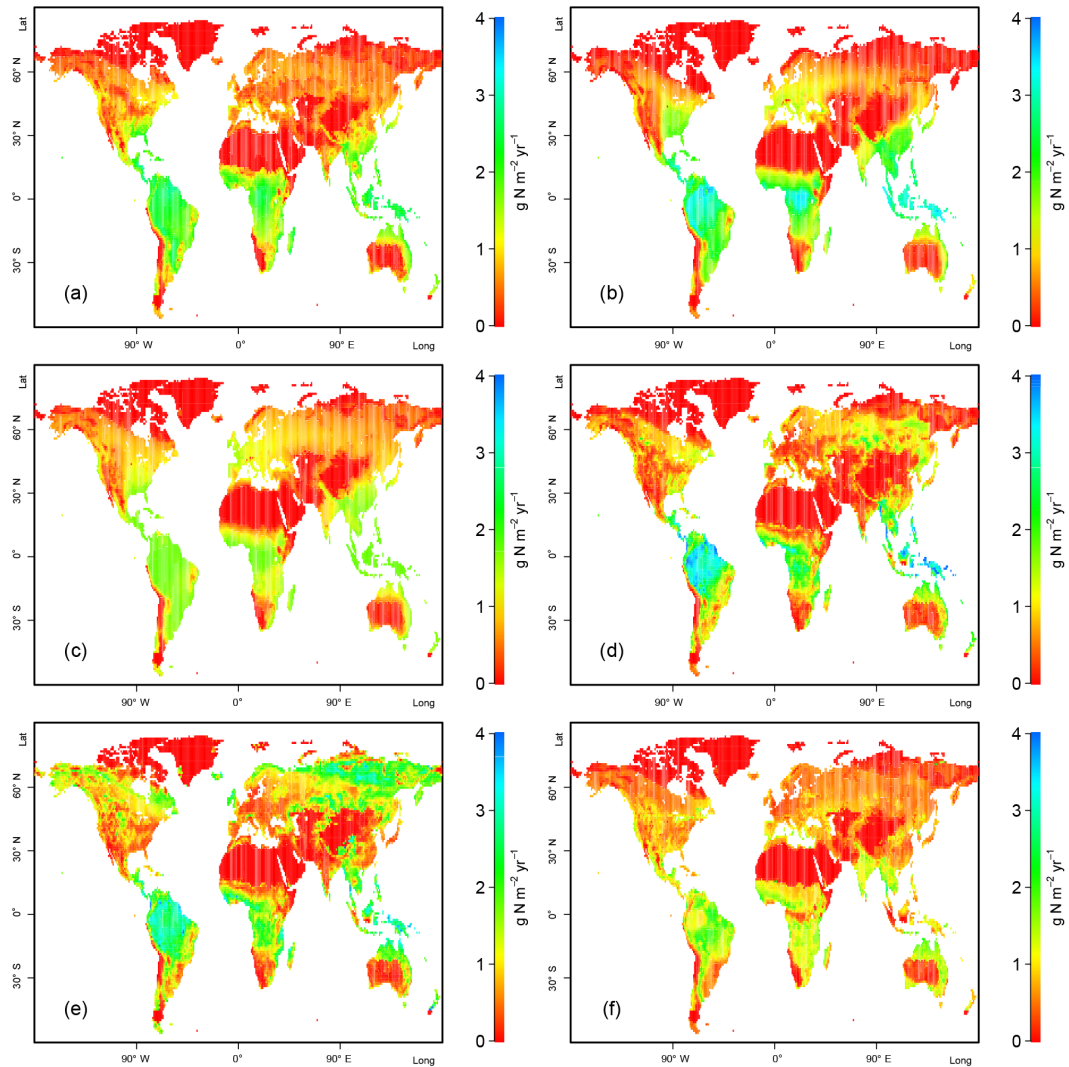


Figure B1. Global biological nitrogen (N) fixation (BNF) rates, as simulated by O-CN applying the six different BNF models for 2000–2013: (a) FOR; (b) AET; (c) PRO; (d) NDT; (e) NDS; (f) OPT.

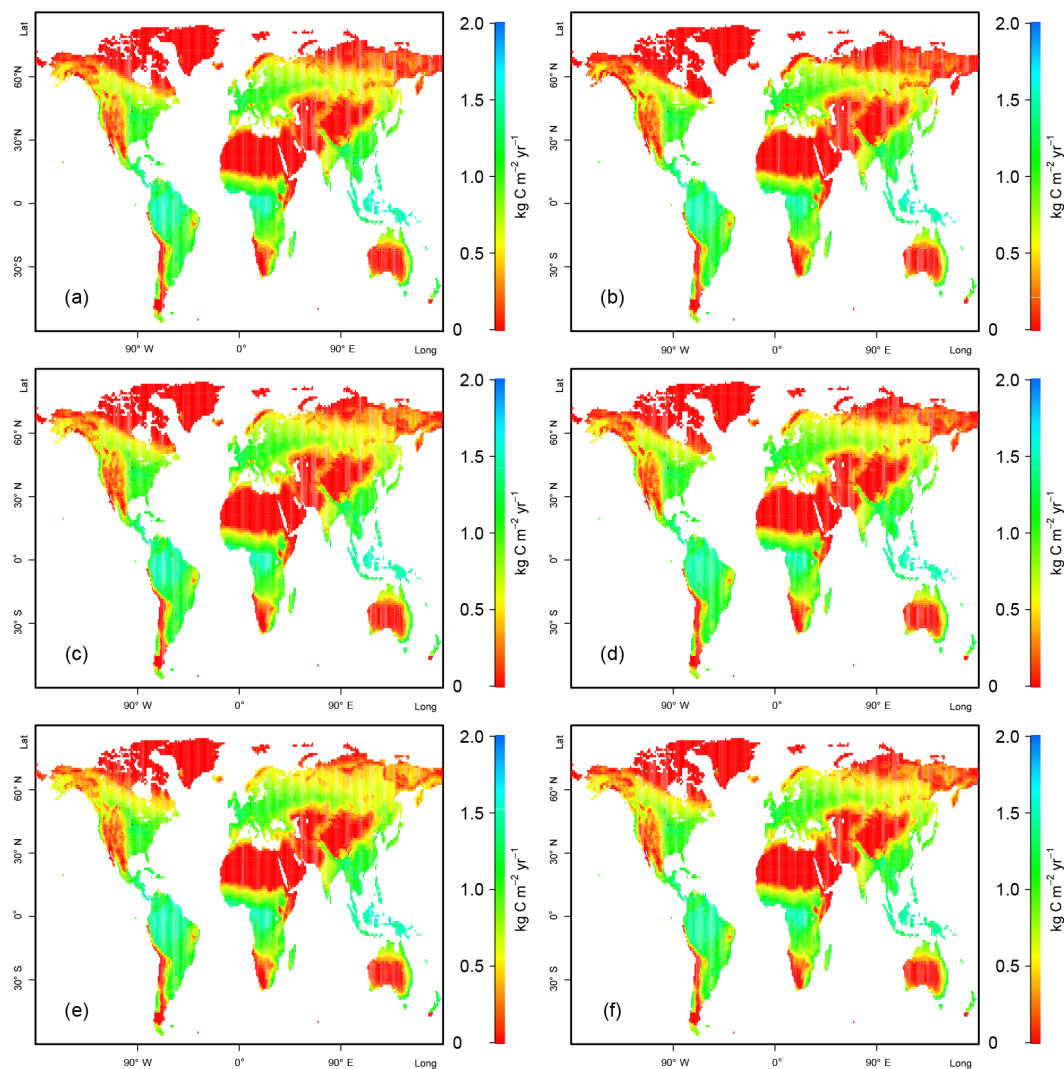


Figure B2. Global net primary productivity (NPP) rates, as simulated by O-CN applying the six different biological nitrogen fixation models for 2000–2013: (a) FOR; (b) AET; (c) PRO; (d) NDT; (e) NDS; (f) OPT.

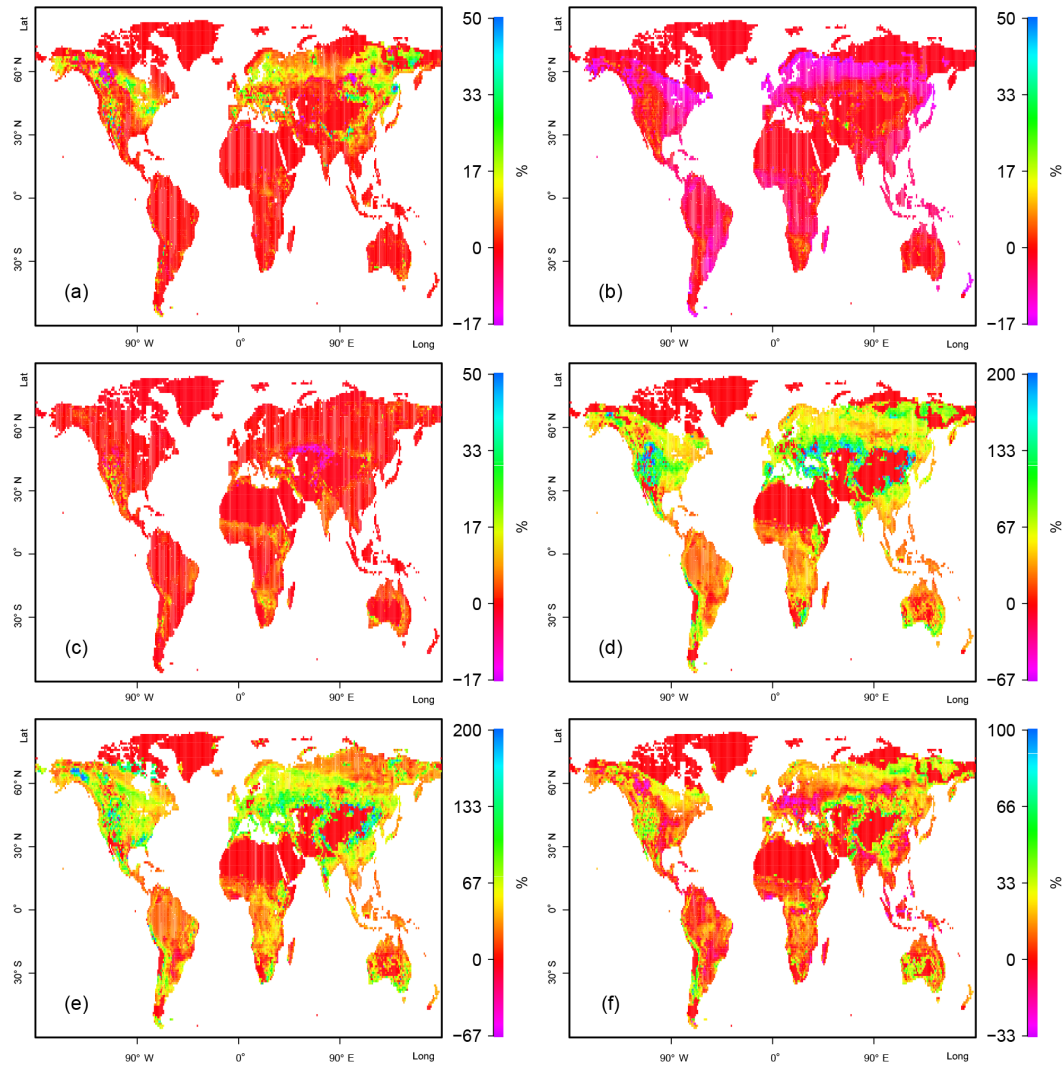


Figure B3. Responses in simulated biological nitrogen (N) fixation (BNF) rates to elevated atmospheric CO₂ concentrations ($e\text{CO}_2$; Fig. 5; $(\text{treatment/control}-1) \times 100$), averaged over the experiment years 140–153: **(a)** FOR; **(b)** AET; **(c)** PRO; **(d)** NDT; **(e)** NDS; **(f)** OPT.

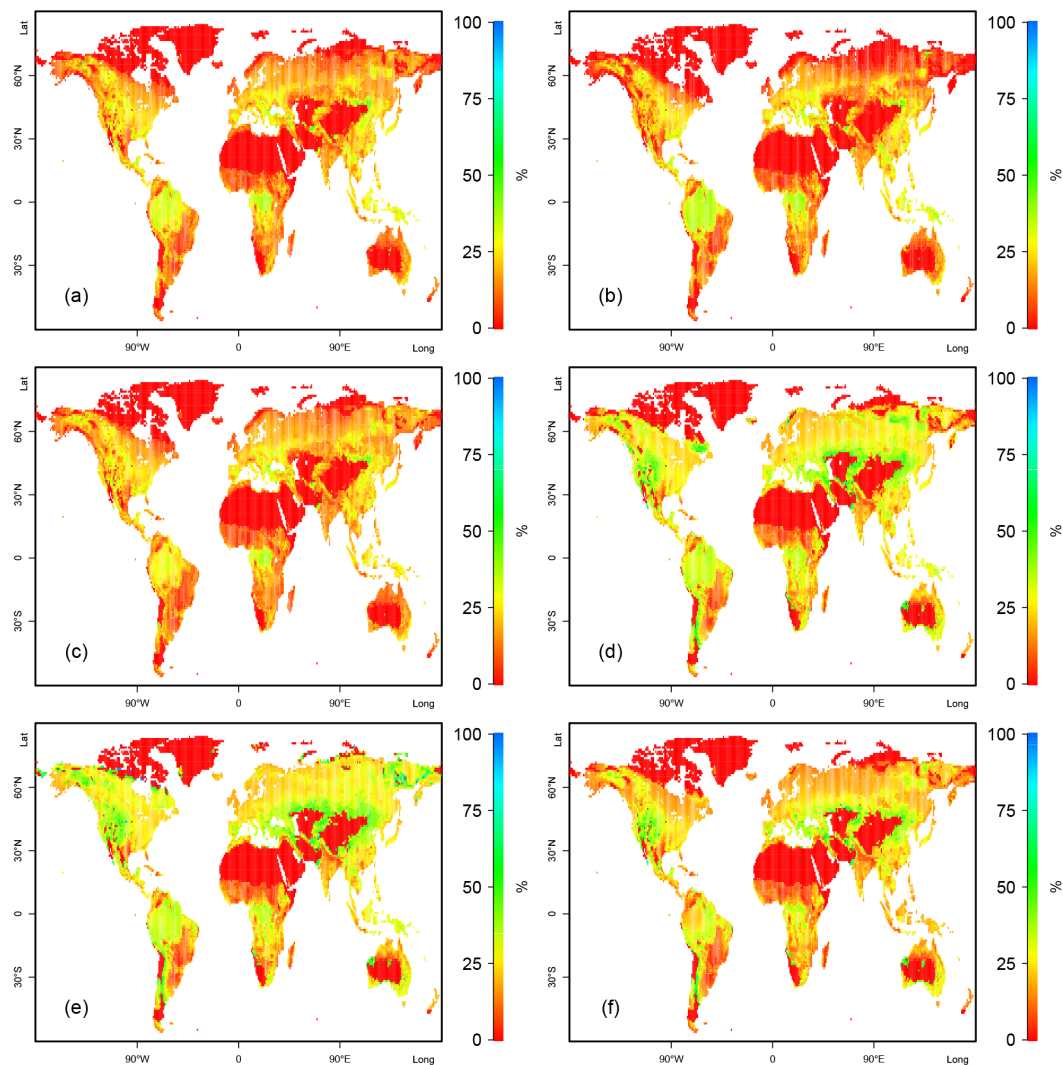


Figure B4. Responses in simulated net primary productivity (NPP) rates to elevated atmospheric CO₂ concentrations ($e\text{CO}_2$; Fig. 5; $(\text{treatment/control}-1) \times 100$), averaged over the experiment years 140–153: (a) FOR; (b) AET; (c) PRO; (d) NDT; (e) NDS; (f) OPT.

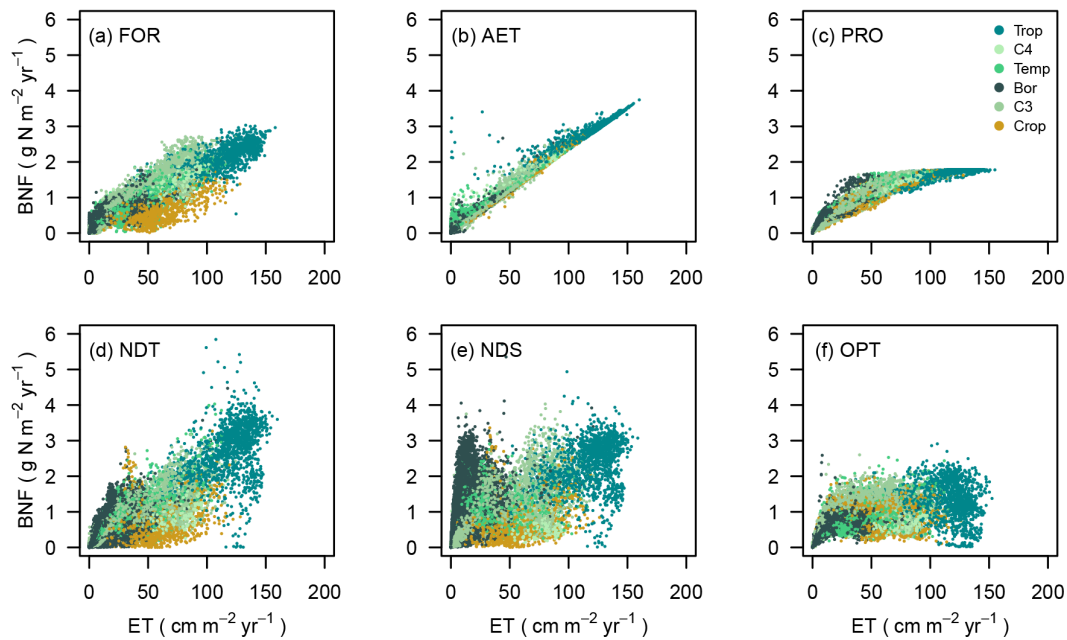


Figure B5. Simulated (simulation A) global relationship between biological nitrogen (N) fixation (BNF) and evapotranspiration (ET), averaged for 2000–2013. Each marker represents one O-CN grid cell. Colours indicate the dominant vegetation type in each grid cell. Trop: tropical forest; C4: C₄ grassland; Temp: temperate forest; Bor: boreal forest; C3: C₃ grassland; Crop: agriculture.

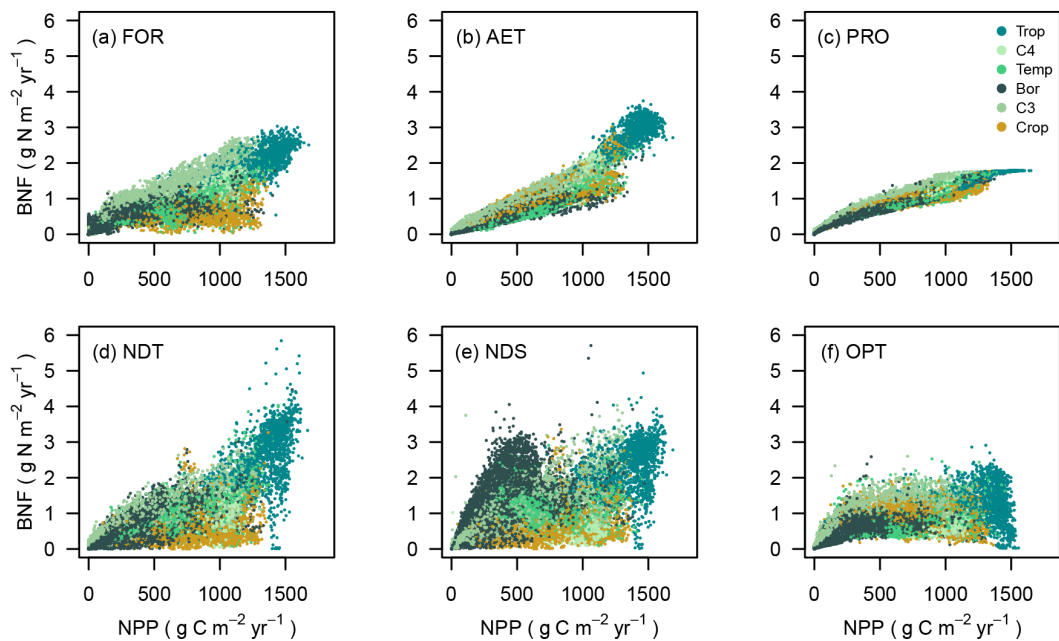


Figure B6. Simulated (simulation A) global relationship between biological nitrogen (N) fixation (BNF) and net primary productivity (NPP), averaged for 2000–2013. Each marker represents one O-CN grid cell. Colours indicate the dominant vegetation type in each grid cell. Trop: tropical forest; C4: C₄ grassland; Temp: temperate forest; Bor: boreal forest; C3: C₃ grassland; Crop: agriculture.

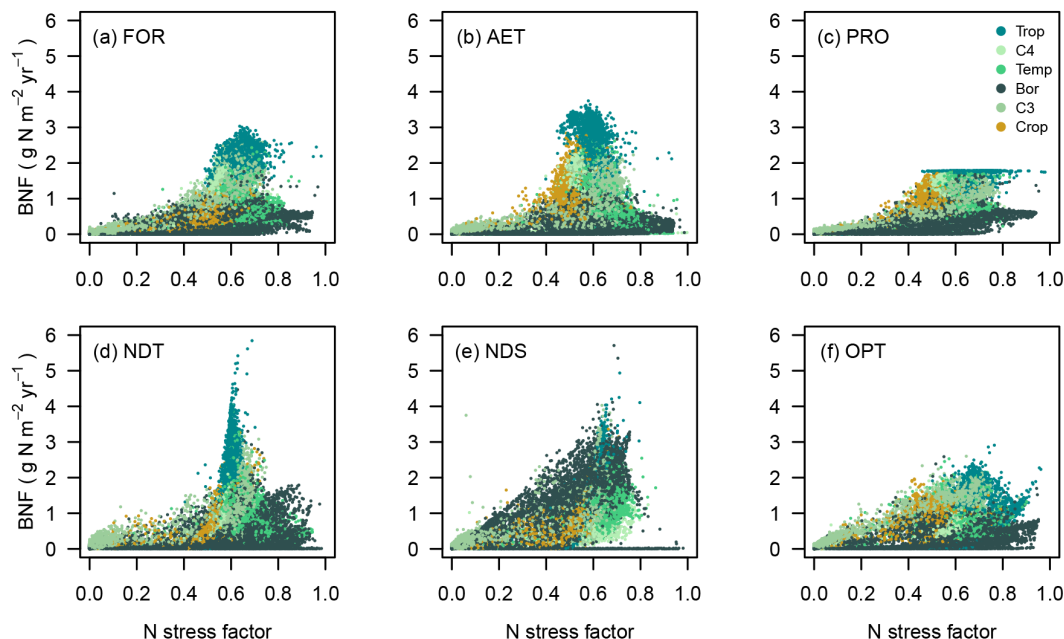


Figure B7. Simulated (A) global relationship between biological nitrogen (N) fixation (BNF) and the relative distance of leaf C : N ratios from the minimal value (“N stress factor”), averaged for 2000–2013. Each marker represents one O-CN grid cell. Colours indicate the dominant vegetation type in each grid cell. Trop: tropical forest; C4: C₄ grassland; Temp: temperate forest; Bor: boreal forest; C3: C₃ grassland; Crop: agriculture.

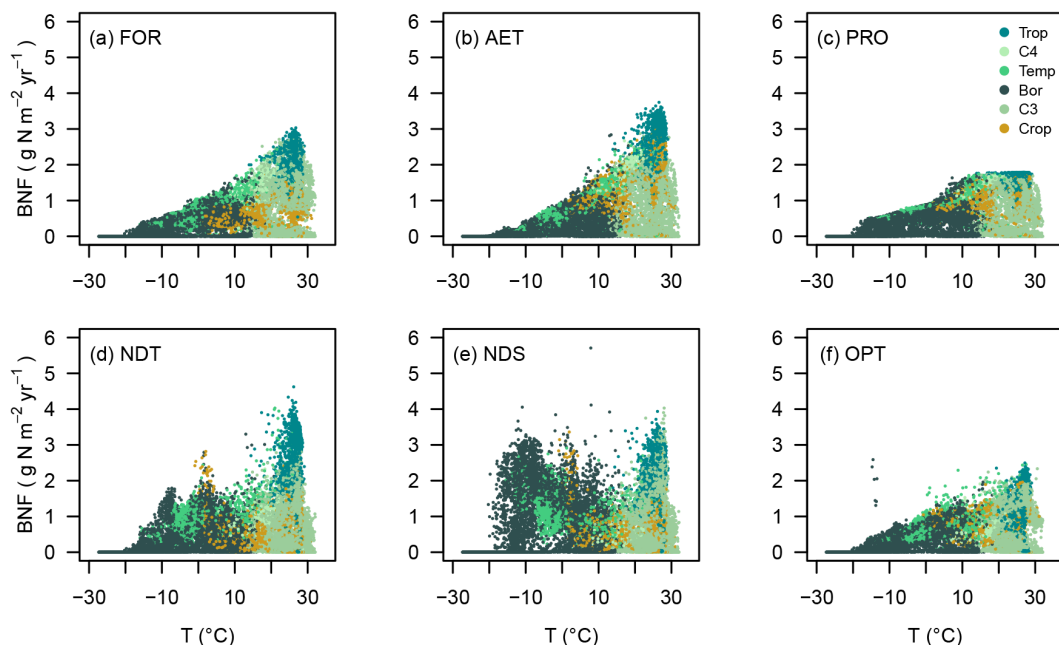


Figure B8. Simulated (A) global relationship between biological nitrogen (N) fixation (BNF) and surface temperature (T), averaged for 2000–2013. Each marker represents one O-CN grid cell. Colours indicate the dominant vegetation type in each grid cell. Trop: tropical forest; C4: C₄ grassland; Temp: temperate forest; Bor: boreal forest; C3: C₃ grassland; Crop: agriculture.

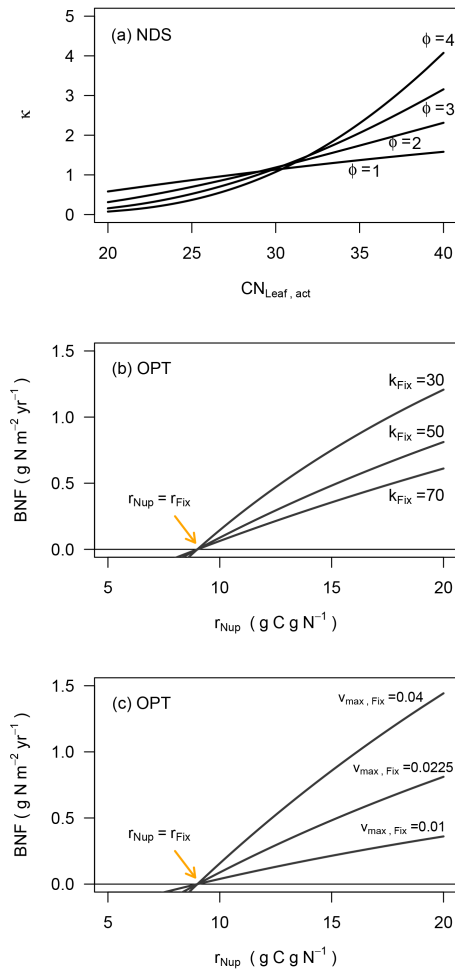


Figure B9. Conceptual parameter sensitivity in the NDS and OPT models. NDS(a): sensitivity of the scaling function κ , which scales plant N demand with plant N status according to Eqs. (A13) and (A14), to variation in the current leaf C:N ratio $CN_{\text{Leaf, act}}$ and the scaling parameter ϕ . We assumed that $CN_{\text{Leaf, min}} = 20$ and $CN_{\text{Leaf, max}} = 40$. OPT(b): sensitivity of BNF ($\text{g N m}^{-2} \text{yr}^{-1}$) to variation in the root N uptake cost r_{Nup} ($\text{g C g}^{-1} \text{N}$) and the half-saturation constant k_{Fix} ($\text{g C g}^{-1} \text{N}$) according to Eq. (A19). C_{root} was fixed at 200 g C m^{-2} , $v_{\text{max, Fix}}$ was fixed at $0.0225 \text{ g N g}^{-1} \text{ C yr}^{-1}$, and r_{Fix} was fixed at $9 \text{ g C g}^{-1} \text{ N}$. The arrow indicates that BNF is zero when $r_{\text{Nup}} = r_{\text{Fix}}$; therefore, variation in r_{Fix} would shift the functions in x direction. OPT(c): sensitivity of BNF to variation in r_{Nup} and the maximum BNF per unit root C, $v_{\text{max, Fix}}$, according to Eq. (A19). C_{root} was fixed at 200 g C m^{-2} , k_{Fix} was fixed at $50 \text{ g C g}^{-1} \text{ N}$, and r_{Fix} was fixed at $9 \text{ g C g}^{-1} \text{ N}$.

Acknowledgements. This work was supported by Microsoft Research through its PhD Scholarship Programme and the European Research Council (ERC) under the European Union's Horizon 2020 research and innovation programme (QUINCY; grant no. 647204). We are grateful to Thomas Hickler for helpful discussion.

The article processing charges for this open-access publication were covered by the Max Planck Society.

Edited by: A. V. Eliseev

References

- Arora, V. K., Boer, G. J., Friedlingstein, P., Eby, M., Jones, C. D., Christian, J. R., Bonan, G., Bopp, L., Brovkin, V., Cadule, P., Hajima, T., Ilyina, T., Lindsay, K., Tjiputra, J. F., and Wu, T.: Carbon–Concentration and Carbon–Climate Feedbacks in CMIP5 Earth System Models, *J. Climate*, 26, 5289–5314, doi:10.1175/jcli-d-12-00494.1, 2013.
- Beer, C., Reichstein, M., Tomelleri, E., Ciais, P., Jung, M., Carvalhais, N., Rödenbeck, C., Altaf Arain, M., Baldocchi, D., Bonan, G. B., Bondeau, A., Cescatti, A., Lasslop, G., Lindroth, A., Lomas, M., Luysaert, S., Margolis, H., Oleson, K. W., Rouspard, O., Veenendaal, E., Viovy, N., Williams, C., Woodward, F. I., and Papale, D.: Terrestrial gross carbon dioxide uptake: Global distribution and covariation with climate, *Science*, 329, 834–838, doi:10.1126/science.1184984, 2010.
- Bonan, G. B.: Forests and climate change: forcings, feedbacks, and the climate benefits of forests, *Science*, 320, 1444–1449, doi:10.1126/science.1155121, 2008.
- Boyer, E. W., Howarth, R. W., Galloway, J. N., Dentener, F. J., Green, P. A., and Vörösmarty, C. J.: Riverine nitrogen export from the continents to the coasts, *Global Biogeochem. Cy.*, 20, GB1S91, doi:10.1029/2005gb002537, 2006.
- Ciais, P., Sabine, C., Bala, G., Bopp, L., Brovkin, V., Canadell, J., Chhabra, A., DeFries, R., Galloway, J., Heimann, M., Jones, C., Le Queiré, C., Myneni, R. B., Piao, S., and Thornton, P.: Carbon and Other Biogeochemical Cycles, in: *Climate Change 2013: The Physical Science Basis. Contribution of Working Group I to the Fifth Assessment Report of the Intergovernmental Panel on Climate Change*, edited by: Stocker, T. F., Qin, D., Plattner, G.-K., Tignor, M., Allen, S. K., Boschung, J., Nauels, A., Xia, Y., Bex, V., and Midgley, P. M., Cambridge University Press, Cambridge, United Kingdom and New York, NY, USA, 465–570, 2013.
- Cleveland, C. C., Townsend, A. R., Schimel, D. S., Fisher, H., Howarth, R. W., Hedin, L. O., Perakis, S. S., Latty, E. F., Von Fischer, J. C., Elseroad, A., and Wasson, M. F.: Global patterns of terrestrial biological nitrogen (N_2) fixation in natural ecosystems, *Global Biogeochem. Cy.*, 13, 623–645, doi:10.1029/1999gb900014, 1999.
- Dufresne, J. L., Foujols, M. A., Denvil, S., Caubel, A., Marti, O., Aumont, O., Balkanski, Y., Bekki, S., Bellenger, H., Benshila, R., Bony, S., Bopp, L., Braconnot, P., Brockmann, P., Cadule, P., Cheruy, F., Codron, F., Cozic, A., Cugnet, D., Noblet, N., Duvel, J. P., Ethé, C., Fairhead, L., Fichefet, T., Flavoni, S., Friedlingstein, P., Grandpeix, J. Y., Guez, L., Guilyardi, E., Hauglustaine, D., Hourdin, F., Idelkadi, A., Ghattas, J., Joussaume, S., Kageyama, M., Krinner, G., Labetoulle, S., Lahellec, A., Lefebvre, M. P., Lefevre, F., Levy, C., Li, Z. X., Lloyd, J., Lott, F., Madec, G., Mancip, M., Marchand, M., Masson, S., Meurdesoif, Y., Mignot, J., Musat, I., Parouty, S., Polcher, J., Rio, C., Schulz, M., Swingedouw, D., Szopa, S., Talandier, C., Terray, P., Viovy, N., and Vuichard, N.: Climate change projections using the IPSL-CM5 Earth System Model: from CMIP3 to CMIP5, *Clim. Dynam.*, 40, 2123–2165, doi:10.1007/s00382-012-1636-1, 2013.
- Dybzinski, R., Farrior, C. E., and Pacala, S. W.: Increased forest carbon storage with increased atmospheric CO_2 despite nitrogen limitation: a game-theoretic allocation model for trees in competition for nitrogen and light, *Glob. Change Biol.*, 21, 1182–1196, doi:10.1111/gcb.12783, 2015.
- Elbert, W., Weber, B., Burrows, S., Steinkamp, J., Büdel, B., Andreae, M. O., and Pöschl, U.: Contribution of cryptogamic covers to the global cycles of carbon and nitrogen, *Nat. Geosci.*, 5, 459–462, doi:10.1038/NGEO1486, 2012.
- Etheridge, D. M., Steele, L. P., Langenfelds, R. L., Francey, R. J., Barnola, J. M., and Morgan, V. I.: Natural and anthropogenic changes in atmospheric CO_2 over the last 1000 years from air in Antarctic ice and firn, *J. Geophys. Res.*, 101, 4115, doi:10.1029/95jd03410, 1996.
- Fisher, J. B., Sitch, S., Malhi, Y., Fisher, R. A., Huntingford, C., and Tan, S. Y.: Carbon cost of plant nitrogen acquisition: A mechanistic, globally applicable model of plant nitrogen uptake, retranslocation, and fixation, *Global Biogeochem. Cy.*, 24, GB1014, doi:10.1029/2009gb003621, 2010.
- Franklin, O., Nasholm, T., Hogberg, P., and Hogberg, M. N.: Forests trapped in nitrogen limitation—an ecological market perspective on ectomycorrhizal symbiosis, *New Phytol.*, 203, 657–666, doi:10.1111/nph.12840, 2014.
- Friedlingstein, P., Cox, P., Betts, R., Bopp, L., Von Bloh, W., Brovkin, V., Cadule, P., Doney, S., Eby, M., Fung, I., Bala, G., John, J., Jones, C., Joos, F., Kato, T., Kawamiya, M., Knorr, W., Lindsay, K., Matthews, H. D., Raddatz, T., Rayner, P., Reick, C., Roeckner, E., Schnitzler, K.-G., Schnur, R., Strassmann, K., Weaver, A. J., Yoshikawa, C., and Zeng, N.: Climate-Carbon Cycle Feedback Analysis: Results from the C⁴MIP Model Intercomparison, *J. Climate*, 19, 3337–3353, doi:10.1175/JCLI3800.1, 2006.
- Galloway, J. N., Dentener, F. J., Capone, D. G., Boyer, E. W., Howarth, R. W., Seitzinger, S. P., Asner, G. P., Cleveland, C. C., Green, P. A., Holland, E. A., Karl, D. M., Michaels, A. F., Porter, J. H., Townsend, A. R., and Vöörsmarty, C. J.: Nitrogen Cycles: Past, Present, and Future, *Biogeochemistry*, 70, 153–226, doi:10.1007/s10533-004-0370-0, 2004.
- Gerber, S., Hedin, L. O., Oppenheimer, M., Pacala, S. W., and Shevliakova, E.: Nitrogen cycling and feedbacks in a global dynamic land model, *Global Biogeochem. Cy.*, 24, GB1001, doi:10.1029/2008gb003336, 2010.
- Goldewijk, K. K.: Estimating global land use change over the past 300 years: The HYDE Database, *Global Biogeochem. Cy.*, 15, 417–433, doi:10.1029/1999gb001232, 2001.
- Goll, D. S., Brovkin, V., Parida, B. R., Reick, C. H., Kattge, J., Reich, P. B., van Bodegom, P. M., and Niinemets, Ü.: Nutrient limitation reduces land carbon uptake in simulations with a model of combined carbon, nitrogen and phosphorus cycling, *Biogeosciences*, 9, 3547–3569, doi:10.5194/bg-9-3547-2012, 2012.

- Gregory, J. M., Jones, C. D., Cadule, P., and Friedlingstein, P.: Quantifying Carbon Cycle Feedbacks, *J. Climate*, 22, 5232–5250, doi:10.1175/2009jcli2949.1, 2009.
- Gruber, N. and Galloway, J. N.: An Earth-system perspective of the global nitrogen cycle, *Nature*, 451, 293–296, doi:10.1038/nature06592, 2008.
- Gutschick, V. P.: Evolved strategies in nitrogen acquisition by plants, *Am. Nat.*, 118, 607–637, doi:10.1086/283858, 1981.
- Hartwig, U. A., Lüscher, A., Daepf, M., Blum, H., Soussana, J.-F., and Nösberger, J.: Due to symbiotic N₂ fixation, five years of elevated atmospheric pCO₂ had no effect on the N concentration of plant litter in fertile, mixed grassland, *Plant Soil*, 224, 43–50, doi:10.1023/A:1004601915836, 2000.
- Hofmöckel, K. S. and Schlesinger, W. H.: Carbon Dioxide Effects on Heterotrophic Dinitrogen Fixation in a Temperate Pine Forest, *Soil Sci. Soc. Am. J.*, 71, 140–144, doi:10.2136/sssaj2006.110, 2007.
- Houlton, B. Z., Wang, Y. P., Vitousek, P. M., and Field, C. B.: A unifying framework for dinitrogen fixation in the terrestrial biosphere, *Nature*, 454, 327–330, doi:10.1038/nature07028, 2008.
- Huang, Y. and Gerber, S.: Global soil nitrous oxide emissions in a dynamic carbon-nitrogen model, *Biogeosciences*, 12, 6405–6427, doi:10.5194/bg-12-6405-2015, 2015.
- Hungate, B., Dukes, J. S., Shaw, M. R., Luo, Y. Q., and Field, C. B.: Nitrogen and Climate Change, *Science*, 302, 1512–1513, doi:10.1126/science.1091390, 2003.
- Hungate, B. A., Stiling, P. D., Dijkstra, P., Johnson, D. W., Ketterer, M. E., Hymus, G. J., Hinkle, C. R., and Drake, B. G.: CO₂ Elicits Long-Term Decline in Nitrogen Fixation, *Science*, 304, 1291, doi:10.1126/science.1095549, 2004.
- Hungate, B. A., Duval, B. D., Dijkstra, P., Johnson, D. W., Ketterer, M. E., Stiling, P., Cheng, W., Millman, J., Hartley, A., and Stover, D. B.: Nitrogen inputs and losses in response to chronic CO₂ exposure in a subtropical oak woodland, *Biogeosciences*, 11, 3323–3337, doi:10.5194/bg-11-3323-2014, 2014.
- Jung, M., Henkel, K., Herold, M., and Churkina, G.: Exploiting synergies of global land cover products for carbon cycle modeling, *Remote Sens. Environ.*, 101, 534–553, doi:10.1016/j.rse.2006.01.020, 2006.
- Krinner, G., Viovy, N., de Noblet-Ducoudré, N., Ogée, J., Polcher, J., Friedlingstein, P., Ciais, P., Sitch, S., and Prentice, I. C.: A dynamic global vegetation model for studies of the coupled atmosphere-biosphere system, *Global Biogeochem. Cy.*, 19, GB1015, doi:10.1029/2003gb002199, 2005.
- Lamarque, J.-F., Bond, T. C., Eyring, V., Granier, C., Heil, A., Klimont, Z., Lee, D., Lioussé, C., Mieville, A., Owen, B., Schultz, M. G., Shindell, D., Smith, S. J., Stehfest, E., Van Aardenne, J., Cooper, O. R., Kainuma, M., Mahowald, N., McConnell, J. R., Naik, V., Riahi, K., and van Vuuren, D. P.: Historical (1850–2000) gridded anthropogenic and biomass burning emissions of reactive gases and aerosols: methodology and application, *Atmos. Chem. Phys.*, 10, 7017–7039, doi:10.5194/acp-10-7017-2010, 2010.
- Li, C., Aber, J., Stange, F., Butterbach-Bahl, K., and Papen, H.: A process-oriented model of N₂O and NO emissions from forest soils: 1. Model development, *J. Geophys. Res.*, 105, 4369–4384, doi:10.1029/1999jd900949, 2000.
- Lüscher, A., Hartwig, U. A., Suter, D., and Nösberger, J.: Direct evidence that symbiotic N₂ fixation in fertile grassland is an important trait for a strong response of plants to elevated atmospheric CO₂, *Glob. Change Biol.*, 6, 655–662, doi:10.1046/j.1365-2486.2000.00345.x, 2000.
- McCarthy, H. R., Oren, R., Johnsen, K. H., Gallet-Budynek, A., Pritchard, S. G., Cook, C. W., Ladeau, S. L., Jackson, R. B., and Finzi, A. C.: Re-assessment of plant carbon dynamics at the Duke free-air CO₂ enrichment site: interactions of atmospheric [CO₂] with nitrogen and water availability over stand development, *New Phytol.*, 185, 514–528, doi:10.1111/j.1469-8137.2009.03078.x, 2010.
- Menge, D. N., Levin, S. A., and Hedin, L. O.: Evolutionary trade-offs can select against nitrogen fixation and thereby maintain nitrogen limitation, *P. Natl. Acad. Sci. USA*, 105, 1573–1578, doi:10.1073/pnas.0711411105, 2008.
- Meyerholt, J. and Zaehle, S.: The role of stoichiometric flexibility in modelling forest ecosystem responses to nitrogen fertilization, *New Phytol.*, 208, 1042–1055, doi:10.1111/nph.13547, 2015.
- Moss, R. H., Edmonds, J. A., Hibbard, K. A., Manning, M. R., Rose, S. K., van Vuuren, D. P., Carter, T. R., Emori, S., Kainuma, M., Kram, T., Meehl, G. A., Mitchell, J. F., Nakicenovic, N., Riahi, K., Smith, S. J., Stouffer, R. J., Thomson, A. M., Weyant, J. P., and Wilbanks, T. J.: The next generation of scenarios for climate change research and assessment, *Nature*, 463, 747–756, doi:10.1038/nature08823, 2010.
- Norby, R. J., Warren, J. M., Iversen, C. M., Medlyn, B. E., and McMurtrie, R. E.: CO₂ enhancement of forest productivity constrained by limited nitrogen availability, *P. Natl. Acad. Sci. USA*, 107, 19368–19373, doi:10.1073/pnas.1006463107, 2010.
- Olivier, J. G. J., Bouwman, A. F., Van der Hoek, K. W., and Berdowski, J. J. M.: Global air emission inventories for anthropogenic sources of NO_x, NH₃ and N₂O in 1990, *Environ. Pollut.*, 102, 135–148, doi:10.1016/S0269-7491(98)80026-2, 1998.
- Parton, W. J., Scurlock, J. M. O., Ojima, D. S., Gilmanov, T. G., Scholes, R. J., Schimel, D. S., Kirchner, T., Menaut, J. C., Seastedt, T., Garcia Moya, E., Kamnalrut, A., and Kinyamario, J. I.: Observations and modeling of biomass and soil organic matter dynamics for the grassland biome worldwide, *Global Biogeochem. Cy.*, 7, 785–809, doi:10.1029/93gb02042, 1993.
- Postgate, J. R.: Biological Nitrogen Fixation, *Nature*, 226, 25–27, doi:10.1038/226025a0, 1970.
- Prentice, I. C., Sykes, M. T., and Cramer, W.: A simulation model for the transient effects of climate change on forest landscapes, *Ecol. Model.*, 65, 51–70, doi:10.1016/0304-3800(93)90126-D, 1993.
- Rastetter, E. B., Vitousek, P. M., Field, C., Shaver, G. R., Herbert, D., and Agren, G. I.: Resource Optimization and Symbiotic Nitrogen Fixation, *Ecosystems*, 4, 369–388, doi:10.1007/s10021-001-0018-z, 2001.
- Reed, S. C., Yang, X., and Thornton, P. E.: Incorporating phosphorus cycling into global modeling efforts: a worthwhile, tractable endeavor, *New Phytol.*, 208, 324–329, doi:10.1111/nph.13521, 2015.
- Saugier, B. and J. Roy: Estimations of global terrestrial productivity: Converging towards a single number?, in: *Global Terrestrial Productivity: Past, Present and Future*, edited by: Mooney, H., Roy, J., and Saugier, B., Academic Press, San Diego, California, doi:10.1016/B978-012505290-0/50024-7, 2001.
- Schimel, D. S., Braswell, B. H., McKeown, R., Ojima, D. S., Parton, W. J., and Pulliam, W.: Climate and nitrogen controls on the

- geography and timescales of terrestrial biogeochemical cycling, *Global Biogeochem. Cy.*, 10, 677–692, doi:10.1029/96gb01524, 1996.
- Sitch, S., Friedlingstein, P., Gruber, N., Jones, S. D., Murray-Tortarolo, G., Ahlström, A., Doney, S. C., Graven, H., Heinze, C., Huntingford, C., Levis, S., Levy, P. E., Lomas, M., Poulter, B., Viovy, N., Zaehle, S., Zeng, N., Arneth, A., Bonan, G., Bopp, L., Canadell, J. G., Chevallier, F., Ciais, P., Ellis, R., Gloor, M., Peylin, P., Piao, S. L., Le Quéré, C., Smith, B., Zhu, Z., and Myrneni, R.: Recent trends and drivers of regional sources and sinks of carbon dioxide, *Biogeosciences*, 12, 653–679, doi:10.5194/bg-12-653-2015, 2015.
- Sokolov, A. P., Kicklighter, D. W., Melillo, J. M., Felzer, B. S., Schlosser, C. A., and Cronin, T. W.: Consequences of considering carbon-nitrogen interactions on the feedbacks between climate and the terrestrial carbon cycle, *J. Climate*, 21, 3776–3796, doi:10.1175/2008jcli2038.1, 2008.
- Smith, B., Wårlind, D., Arneth, A., Hickler, T., Leadley, P., Siltberg, J., and Zaehle, S.: Implications of incorporating N cycling and N limitations on primary production in an individual-based dynamic vegetation model, *Biogeosciences*, 11, 2027–2054, doi:10.5194/bg-11-2027-2014, 2014.
- Smith, M. J., Purves, D. W., Vanderwel, M. C., Lyutsarev, V., and Emmott, S.: The climate dependence of the terrestrial carbon cycle, including parameter and structural uncertainties, *Biogeosciences*, 10, 583–606, doi:10.5194/bg-10-583-2013, 2013.
- Stocker, B. D., Roth, R., Joos, F., Spahni, R., Steinacher, M., Zaehle, S., Bouwman, L., Xu, R. I., and Prentice, I. C.: Multiple greenhouse-gas feedbacks from the land biosphere under future climate change scenarios, *Nature Climate Change*, 3, 666–672, doi:10.1038/nclimate1864, 2013.
- Sullivan, B. W., Smith, W. K., Townsend, A. R., Nasto, M. K., Reed, S. C., Chazdon, R. L., and Cleveland, C. C.: Spatially robust estimates of biological nitrogen (N) fixation imply substantial human alteration of the tropical N cycle, *P. Natl. Acad. Sci. USA*, 111, 8101–8106, doi:10.1073/pnas.1320646111, 2014.
- Thomas, R. Q., Brookshire, E. N., and Gerber, S.: Nitrogen limitation on land: how can it occur in Earth system models?, *Glob. Change Biol.*, 21, 1777–1893, doi:10.1111/gcb.12813, 2015.
- Thornton, P. E., Lamarque, J.-F., Rosenbloom, N. A., and Mahowald, N. M.: Influence of carbon-nitrogen cycle coupling on land model response to CO₂ fertilization and climate variability, *Global Biogeochem. Cy.*, 21, GB4018, doi:10.1029/2006gb002868, 2007.
- Vitousek, P. M. and Field, C. B.: Ecosystem constraints to symbiotic nitrogen fixers: a simple model and its implications, *Biogeochemistry*, 46, 179–202, doi:10.1007/BF01007579, 1999.
- Vitousek, P. M. and Howarth, R. W.: Nitrogen limitation on land and in the sea: How can it occur?, *Biogeochemistry*, 13, 87–115, doi:10.1007/bf00002772, 1991.
- Vitousek, P. M., Cassman, K., Cleveland, C., Crews, T., Field, C. B., Grimm, N. B., Howarth, R. W., Marino, R., Martinelli, L., Rastetter, E. B., and Sprent, J. I.: Towards an ecological understanding of biological nitrogen fixation, *Biogeochemistry*, 57, 1–45, doi:10.1023/A:1015798428743, 2002.
- Vitousek, P. M., Menge, D. N., Reed, S. C., and Cleveland, C. C.: Biological nitrogen fixation: rates, patterns and ecological controls in terrestrial ecosystems, *Philos. T. R. Soc. Lon.*, 368, 20130119, doi:10.1098/rstb.2013.0119, 2013.
- Wang, Y.-P. and Houlton, B. Z.: Nitrogen constraints on terrestrial carbon uptake: Implications for the global carbon-climate feedback, *Geophys. Res. Lett.*, 36, L24403, doi:10.1029/2009gl041009, 2009.
- Wang, Y. P., Houlton, B. Z., and Field, C. B.: A model of biogeochemical cycles of carbon, nitrogen, and phosphorus including symbiotic nitrogen fixation and phosphatase production, *Global Biogeochem. Cy.*, 21, GB1018, doi:10.1029/2006gb002797, 2007.
- Wang, Y. P., Law, R. M., and Pak, B.: A global model of carbon, nitrogen and phosphorus cycles for the terrestrial biosphere, *Biogeosciences*, 7, 2261–2282, doi:10.5194/bg-7-2261-2010, 2010.
- Wania, R., Meissner, K. J., Eby, M., Arora, V. K., Ross, I., and Weaver, A. J.: Carbon-nitrogen feedbacks in the UVic ESCM, *Geosci. Model Dev.*, 5, 1137–1160, doi:10.5194/gmd-5-1137-2012, 2012.
- Welp, L. R., Keeling, R. F., Meijer, H. A., Bollenbacher, A. F., Piper, S. C., Yoshimura, K., Francey, R. J., Allison, C. E., and Wahlen, M.: Interannual variability in the oxygen isotopes of atmospheric CO₂ driven by El Niño, *Nature*, 477, 579–582, doi:10.1038/nature10421, 2011.
- Wieder, W. R., Cleveland, C. C., Lawrence, D. M., and Bonan, G. B.: Effects of model structural uncertainty on carbon cycle projections: biological nitrogen fixation as a case study, *Environ. Res. Lett.*, 10, 044016, doi:10.1088/1748-9326/10/4/044016, 2015.
- Xu, R. I. and Prentice, I. C.: Terrestrial nitrogen cycle simulation with a dynamic global vegetation model, *Glob. Change Biol.*, 14, 1745–1764, doi:10.1111/j.1365-2486.2008.01625.x, 2008.
- Yang, X., Wittig, V., Jain, A. K., and Post, W.: Integration of nitrogen cycle dynamics into the Integrated Science Assessment Model for the study of terrestrial ecosystem responses to global change, *Global Biogeochem. Cy.*, 23, GB4029, doi:10.1029/2009gb003474, 2009.
- Zaehle, S.: Terrestrial nitrogen-carbon cycle interactions at the global scale, *Philos. T. R. Soc. B*, 368, 20130125, doi:10.1098/rstb.2013.0125, 2013.
- Zaehle, S. and Dalmonech, D.: Carbon–nitrogen interactions on land at global scales: current understanding in modelling climate biosphere feedbacks, *Current Opinion in Environmental Sustainability*, 3, 311–320, doi:10.1016/j.cosust.2011.08.008, 2011.
- Zaehle, S. and Friend, A. D.: Carbon and nitrogen cycle dynamics in the O-CN land surface model: 1. Model description, site-scale evaluation, and sensitivity to parameter estimates, *Global Biogeochem. Cy.*, 24, GB1005, doi:10.1029/2009gb003521, 2010.
- Zaehle, S., Friedlingstein, P., and Friend, A. D.: Terrestrial nitrogen feedbacks may accelerate future climate change, *Geophys. Res. Lett.*, 37, L01401, doi:10.1029/2009gl041345, 2010a.
- Zaehle, S., Friend, A. D., Friedlingstein, P., Dentener, F., Peylin, P., and Schulz, M.: Carbon and nitrogen cycle dynamics in the O-CN land surface model: 2. Role of the nitrogen cycle in the historical terrestrial carbon balance, *Global Biogeochem. Cy.*, 24, GB1006, doi:10.1029/2009gb003522, 2010b.
- Zaehle, S., Ciais, P., Friend, A. D., and Prieur, V.: Carbon benefits of anthropogenic reactive nitrogen offset by nitrous oxide emissions, *Nat. Geosci.*, 4, 601–605, doi:10.1038/ngeo1207, 2011.
- Zaehle, S., Medlyn, B. E., De Kauwe, M. G., Walker, A. P., Dietze, M. C., Hickler, T., Luo, Y., Wang, Y. P., El-Masri, B., Thornton, P., Jain, A., Wang, S., Wårlind, D., Weng, E., Parton, W., Iversen,

C. M., Gallet-Budynek, A., McCarthy, H., Finzi, A., Hanson, P. J., Prentice, I. C., Oren, R., and Norby, R. J.: Evaluation of 11 terrestrial carbon-nitrogen cycle models against observations from two temperate Free-Air CO₂ Enrichment studies, *New Phytol.* 202, 803–822, doi:10.1111/nph.12697, 2014.

Zhang, Q., Wang, Y. P., Matear, R. J., Pitman, A. J., and Dai, Y. J.: Nitrogen and phosphorous limitations significantly reduce future allowable CO₂ emissions, *Geophys. Res. Lett.*, 41, 632–637, doi:10.1002/2013gl058352, 2014.